

Review

# An Overview of Infrared Remote Sensing of Volcanic Activity

**Matthew Blakett**

School of Energy, Construction and Environment, Coventry University, Coventry CV1 5FB, UK;  
m.blakett@coventry.ac.uk

Academic Editors: Carosena Meola and Gonzalo Pajares Martinsanz  
Received: 2 October 2016; Accepted: 6 April 2017; Published: 12 April 2017

**Abstract:** Volcanic activity consists of the transfer of heat from the interior of the Earth to the surface. The characteristics of the heat emitted relate directly to the geological processes underway and can be observed from space, using the thermal sensors present on many Earth-orbiting satellites. For over 50 years, scientists have utilised such sensors and are now able to determine the sort of volcanic activity being displayed without hazardous and costly field expeditions. This review will describe the theoretical basis of the discipline and then discuss the sensors available and the history of their use. Challenges and opportunities for future developments are then discussed.

**Keywords:** infrared remote sensing; volcanoes; Earth observation; satellites

---

## 1. Introduction

Remote sensing is the observation of an object without requiring contact with the object being observed. It is something the human eye does all of the time, and humans have also developed specialist equipment for the purpose, ranging from the simple camera, which detects reflected electromagnetic radiation (in this case, from the visible portion of the spectrum), to complex sensors, which detect electromagnetic radiation in other portions of the spectrum, including in the infrared. In its application to volcanic activity, arguably the chief advantage of infrared remote sensing, as opposed to remote sensing in the visual portion of the spectrum, is that it detects the electromagnetic emissions of hot volcanic surfaces themselves, which are a function of the temperature and emissivity of the surface, as opposed to detecting the electromagnetic radiation, which has simply been reflected from the surface.

Observations in the infrared region of the spectrum are useful when examining volcanic activity. This is because volcanic activity consists of the transfer of heat from within the Earth to the surface, and observations of this heat often relate directly to the activity of a volcano at a specific time [1]. The activity observed, and expressed in the thermal signature, might be a fresh lava flow or an active lava lake, or may be more subtle, such as a degassing surface or warmed crater-lake. Understanding the activity at a volcanic site using such data is clearly useful in determining a volcano's status and, as such in predicting future activity. Making such observations remotely and at a safe distance is also clearly advantageous.

This review will firstly explain some of the theoretical concepts and considerations that must be taken into account in the infrared remote sensing of volcanic activity. Many of these considerations will be common to other disciplines, but are here framed from the unique perspective of monitoring volcanic activity. The sensors used for volcanic monitoring, and the history of the discipline, will then be discussed. The prospects, opportunities, and even threats, for the discipline in the coming decades will then be highlighted. It should be noted that while infrared remote sensing may be used for monitoring various aspects of volcanism, from heat to gas and ash emissions, the focus of this review is limited to the monitoring of volcanic heat emissions.

## 2. Infrared Remote Sensing: Theory

All objects above 0 K (absolute zero) emit electromagnetic radiation, but the radiant flux density (i.e., rate of energy flow per unit area) and spectral composition of these emissions depend on the temperature of the emitting object. According to the Stefan–Boltzmann law [2,3], the radiant flux density emitted by an object is directly proportional to the fourth power of the object’s surface temperature, meaning that the hotter an object, the greater the total energy it will radiate, and this applies to all wavelengths of emission (see Figure 1). According to Wien’s displacement law [4], the peak wavelength of spectral radiant emissions also becomes shorter with increasing temperature, (also see Figure 1).

The energy radiated from an object, otherwise termed radiant flux, is quantified in terms of radiance per unit of wavelength and is referred to as spectral radiance. The spectral radiance,  $L_{\lambda}(T)$ , (in units of  $W\ m^2\ sr^{-1}\ \mu m^{-1}$ ), emitted by a blackbody at temperature ( $T$ ) and wavelength ( $\lambda$ ), can be calculated using the Planck function [5] below and as represented in Figure 1:

$$L_{\lambda}(T) = \frac{C_1}{\lambda^5 \left( \exp\left(\frac{C_2}{\lambda T}\right) - 1 \right)} \tag{1}$$

where  $C_1$  and  $C_2 =$  constants of  $1.19 \times 10^{-16}$  and  $1.44 \times 10^{-2}$  m K, respectively [6].

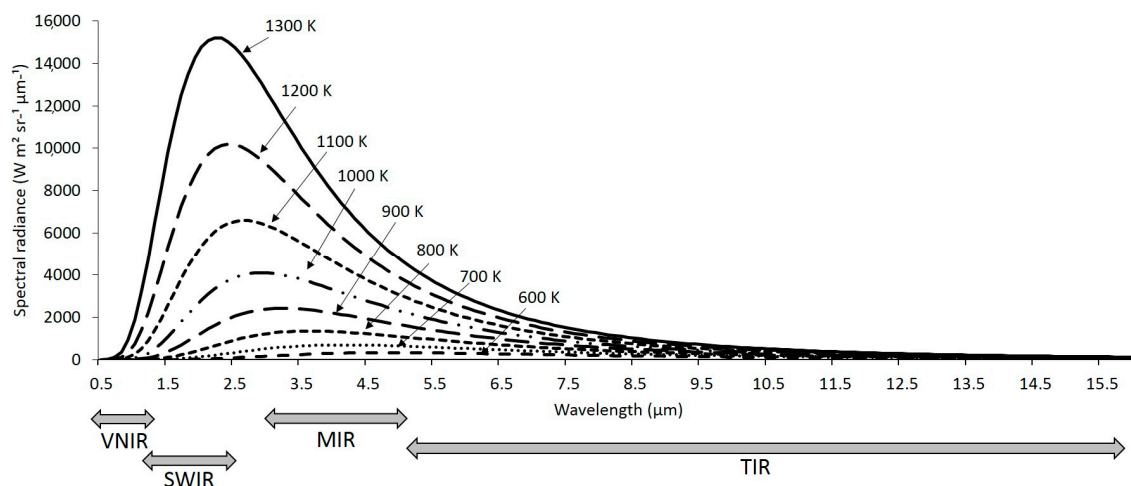


**Figure 1.** Relationship between the spectral radiant emissions (in terms of quantity and wavelength) and temperature of the emitting surface, thus representing the Planck function and both the Stefan–Boltzmann and Wien displacement laws. Different portions of the infrared spectrum are also depicted (VNIR: visual and near infrared; SWIR: short-wave infrared; MIR: mid-infrared; TIR: thermal infrared).

The temperature of volcanic features varies widely. Fresh lava may be between 1073 and 1273 K, although the temperature of lava lakes has been measured at up to 1473 K, while cooler active surfaces may reach 673 K [7,8]. At these temperatures, the chief radiant emissions are in the thermal infrared (TIR), middle infrared (MIR) and shortwave infrared (SWIR) portions of the spectrum (see Figure 1). Various Earth-observing satellites have sensors capable of observing these infrared emissions and as such are routinely used for volcanic observations (Table 1), despite their original purposes often being far removed from such geological applications. One complication, however, is that all components of the Earth’s surface, by virtue of their temperature, also produce detectable radiant emissions in the MIR and TIR portions of the spectrum, and these signals must be removed if those attributable to active volcanism are to be accurately quantified. In contrast, SWIR radiation is only emitted in detectable quantities from very hot surfaces (e.g., fires and incandescent lava), and as such, in nighttime imagery,

such removal steps are not required, although in daytime imagery, reflected solar radiation must be removed from any SWIR signals.

**Table 1.** Characteristics and attributes of the main sensors used for the infrared remote sensing of volcanoes, with abbreviations used in this paper also defined.

Sensor	Characteristics
<b>Advanced Along-Track Scanning Radiometer (AATSR)</b> on-board the European Space Agency (ESA) Envisat satellite	7 bands: VNIR-MIR-TIR Resolution: 1000 m
<b>Advanced Land Imager (ALI)</b> on-board the NASA Earth Observation (EO)-1 satellite	9 bands: VNIR-SWIR Resolution: 30 m
<b>Advanced Spaceborne Thermal Emission and Reflection Radiometer (ASTER)</b> on-board NASA Terra	14 bands: VNIR-SWIR-TIR Resolution: 15, 30 and 90 m
<b>Along Track Scanning Radiometer (ATSR)-1 and ATSR-2</b> on-board the ESA European Remote Sensing (ERS) Satellites	4 bands: SWIR-MIR-TIR Resolution: 1000 m
<b>Advanced Very High Resolution Radiometer (AVHRR)</b> on-board the National Oceanic and Atmospheric Administration (NOAA) satellites	5 bands: VNIR-SWIR-MIR-TIR Resolution: 1100 m
<b>Enhanced Thematic Mapper Plus (ETM+)</b> on-board the NASA Landsat 7 satellite	8 bands: VNIR-SWIR-TIR Resolution: 15, 30 and 60 m
<b>Imager</b> on-board the NASA Geostationary Operational Environmental Satellite (GOES)	5 bands: VNIR-MIR-TIR Resolutions: 1000–4000 m
<b>Hyperion</b> on-board the NASA EO-1 satellite	220 bands: VNIR-SWIR Resolution: 30 m
<b>Meteosat Visible and InfraRed Imager (MVISI)</b> on-board the ESA Meteosat First Generation satellites	3 bands: VIS-TIR Resolutions: 250–5000 m
<b>Moderate-resolution Imaging Spectroradiometer (MODIS)</b> on-board NASA Terra and Aqua satellites	32 bands: VNIR-MIR-TIR Resolutions: 250, 500 and 1000 m
<b>Operational Land Imager (OLI)</b> on-board the NASA Landsat-8 satellite	9 bands: VNIR-SWIR Resolutions: 15–30 m
<b>Optical Sensor (OPS)</b> on-board the Japanese Earth Resources Satellite 1 (JERS-1) satellite	7 bands: VNIR-SWIR Resolution: 18 m × 24 m
<b>Spinning Enhanced Visible &amp; Infrared Imager (SEVERI)</b> on-board the ESA Meteosat Second Generation satellites	12 bands: VNIR-TIR Resolution: 1000–3000 m
<b>Thermal Infrared Sensor (TIRS)</b> on-board the NASA Landsat-8 satellite	2 bands: TIR Resolution: 100 m
<b>Visible Infrared Imaging Radiometer Suite (VIIRS)</b> on board the NASA Suomi National Polar-Orbiting Partnership (S-NPP) satellite	22 bands: VNIR-SWIR-TIR Resolutions: 375–750 m

Early satellites such as the National Aeronautics and Space Administration's (NASA's) Television Infrared Observation Satellite (TIROS) series, launched throughout the 1960s, possessed TIR Earth-observation capabilities for meteorological observations. Since this period, infrared observations have remained crucial for meteorological purposes while also providing an excellent means of observing terrestrial 'hot phenomena', ranging from wildfires to active volcanoes. Some examples of using orbiting infrared sensors for this purpose include [9], in which it was shown that subtle precursory TIR signals could be detected prior to a 2006 eruption of Bezymianny Volcano in Russia and [10], which similarly showed how TIR observations of Bezymianny could be used to monitor the volcano's changing state during a later eruption. More recently, [11] used satellite-retrieved TIR observations, augmented with ground-based observations, to isolate precursory signals, and a subsequent eruption, at Redoubt Volcano in Alaska and [12] demonstrated the utility of satellite TIR observations for determining lava extrusion rates and discriminating different types of lava dome activity, at Merapi Volcano, Indonesia. Likewise, several satellite sensors have MIR detection capabilities, which have been shown to be useful in monitoring both thermally-anomalous volcanic surfaces and, also, those at a more ambient temperature. Wright and Pilger [13,14], for example, utilised MIR bands to quantify the radiant emissions from a number of volcanoes and used the same data

to monitor the variability in heat flux from the lava lake at Mount Erebus in Antarctica, respectively, while [15] demonstrated a volcanic activity detection system that harnesses detected MIR signals.

Some satellite sensors have been equipped with SWIR detection capabilities, in large part because SWIR image data can be used in land surface reflectance studies [16]; in fact, the SWIR bands on ASTER were chosen for the absorption features of various minerals and clays [17,18]. However, such bands are also useful in monitoring hot surfaces, especially at night [19], and until the malfunction in 2008, ASTER was regularly used for such purposes. Comparable functionality has now passed to the largely under-investigated SWIR bands of Landsat-8 [20].

The advantage of SWIR volcanic observations is that, in the absence of sunlight, terrestrial SWIR signals recorded from space will be purely a product of the temperature of a hot emitting surface. In contrast, MIR and TIR detections from space will be the product of emissions from both ambient and hot surface components, the former of which must therefore be removed. The advantage that MIR and TIR observations have over SWIR observations, however, is that they will also detect cooler volcanic surfaces, thereby negating the requirement of incandescent or fresh lava to be present while facilitating the monitoring of a greater range of volcanic activity.

### 3. Specific Considerations for the Infrared Remote Sensing of Volcanic Activity

There are a number of considerations that must be taken into account when acquiring and analysing thermal imagery of volcanic activity, and this section will examine these.

**Spatial resolution:** This term relates to the smallest spatial unit of data that a sensor can collect, and in terms of remote sensing, it relates to the area on the Earth's surface that is imaged by one pixel. It is to some extent a function of the altitude of the sensor, with the area imaged by one pixel being larger the further a sensor is from the surface. Another influence on the pixel size is the type of data being collected, with technological constraints limiting the spatial resolution of longer wavelength sensors. Readers will be familiar with high-resolution Google Earth imagery, which allows small features on Earth's surface to be identified (sometimes features smaller than 1 m in size). Unlike such visual band remote sensing, however, the spatial resolution of infrared imagery is relatively coarse, with the highest resolution that is used for volcanic observations being 30 m (for example, the SWIR bands of NASA's ASTER and Landsat-8 sensors) and with an even coarser resolution for longer wavelength TIR bands (e.g., 1000 m for MODIS). Additionally, even the highest spatial resolution for an infrared sensor currently in orbit is only 5.5 m (the Korea Aerospace Research Institute's Korea Multi-Purpose Satellite, KOMPSAT-3A, [21]). The cause of the disparity in spatial resolution between visual and infrared bands is the higher complexity in optical equipment required for the latter, with cooling of the longer wavelength photon detectors, for example, being necessary, which hinders the development of smaller detector elements [22,23].

The significance of the requirement for larger infrared-imaging pixels is that the area imaged by one MODIS TIR pixel, for example, is rather large (1000 m × 1000 m), and when imaging an active lava-flow, such a pixel will detect radiance from various surface components (i.e., hot-incandescent and cooling lava-flows and even non-volcanic surfaces). As the radiance detected within one pixel is an average of the whole area imaged, with signals from sub-pixel components combined into a one 'pixel-integrated' value [24], the higher the spatial resolution of a sensor (i.e., the smaller the pixel size), the greater the level of accuracy and detail that will be discernible (see Figure 2). In providing a greater level of detail, smaller pixels image a smaller area of Earth's surface, but this has a downside: that any hot surface imaged will constitute a greater proportion of a small pixel's field of view, therefore increasing the possibility of saturation. As such, despite the added detail provided by higher resolution infrared sensors, those of coarser resolution (e.g., 1000 m) remain useful in the remote monitoring of the most radiant volcanic activity.

**Temporal resolution:** The temporal resolution of remotely-sensed data refers to the regularity with which a point on the Earth's surface can be imaged by a sensor, and this, as well as the spatial and temporal resolution of spaceborne remote sensing devices are, in practice, inversely related [25].

The reason for this is that the higher the spatial resolution of a sensor, the smaller its pixels and, therefore, the narrower its swath, where the swath is the width of the area on the Earth’s surface that a sensor scans on overpass (Figure 3). As a narrower swath views less of the Earth’s surface at any one time, it will image the entire surface of the Earth with less regularity, hence reducing the temporal resolution. The swath width of NASA’s OLI, for example, is 185 km, with a pixel size of 30 m, resulting in a temporal resolution, otherwise termed revisit frequency, of 16 days (i.e., it will view the same point on the Earth’s surface, such as a volcano, once every 16 days); NASA’s MODIS, in contrast, has a swath width of 2330 km and pixel size of 1 km, resulting in a twice-daily temporal resolution. A reduced temporal resolution is sub-optimal if instantaneous reports of volcanic activity are required (for this, geostationary satellites may be used), but is often adequate for determining trends in volcanic activity over time.

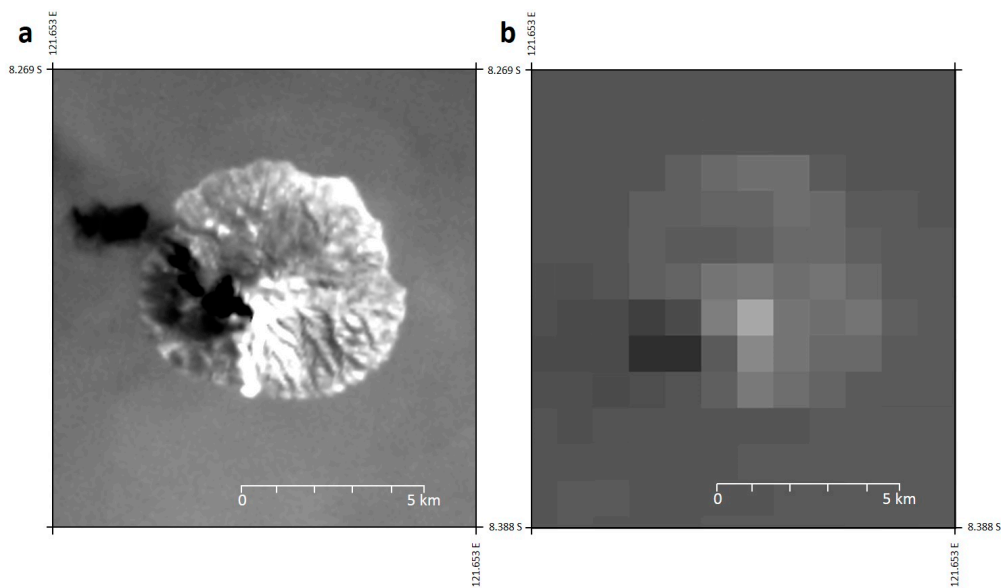


**Figure 2.** Infrared imagery of Palu’e Island, and Paluweh Volcano, Indonesia. (a) Landsat-8 infrared imagery, with a spatial resolution of 30 m, captured 0200 UTC on 29 April 2013; (b) MODIS infrared imagery (Calibrated Earth View data), with a spatial resolution of 1000 m, captured 0210 UTC on 30 April 2013. Note the greater level of detail discernible in (a) compared to (b).

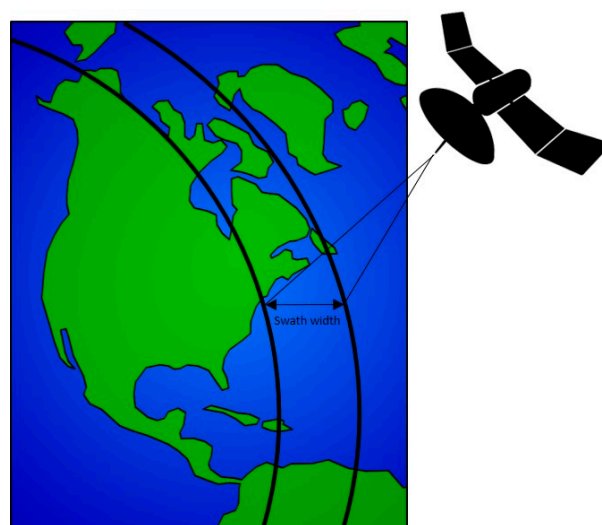


**Figure 3.** The swath width of an Earth Observing satellite sensor.

**Spectral resolution:** This relates to the capacity of a sensor to distinguish different parts of the electromagnetic spectrum and, in many ways, is also inversely related to the spatial and temporal resolution (see Figure 4), with the dictating factor often being the bandwidth of data transfer. NASA's Hypsiri, for example (a sensor that was due for launch 2013–2016, but is likely delayed until 2022 at the earliest [26]), will generate up to 1 GB of data per second of imaging, due to possessing 212 bands in the 380–2500-nm region of the spectrum, and this must all be broadcast to the surface [27,28]. Such large data requirements have necessitated its design with a smaller swath width (150 km for the SWIR bands) to reduce the quantity of data it will produce on each overpass, but in turn, this will reduce its temporal resolution. In contrast, NASA's VIIRS acquires a maximum of 10.5 MB of data per second, and given this, and the fact that it has fewer data-collecting bands, this means that it could be designed with a wider swath (3060 km), so that more of the Earth's surface could be imaged on each overpass, thereby enhancing its temporal resolution.

An additional consideration is that as the spectral (and indeed spatial) resolution increases, the actual signal detected within a band (or pixel) decreases, thereby reducing the signal to noise ratio. This complication adds to the trade-offs represented in Figure 4 that must be weighed by sensor designers and those interpreting such data.

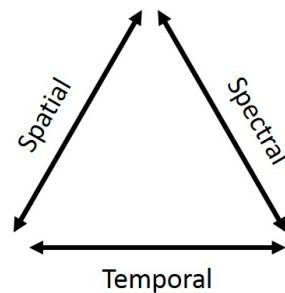


**Figure 4.** The trade-off between spatial, spectral and temporal resolution for Earth observation imagery. These relationships are a function of data transfer bandwidths; assuming a fixed bandwidth, a sensor possessing a high spectral resolution will need to compromise on either spatial or temporal resolution, and so on.

**Orbit:** There are two types of satellite orbits used for volcanic remote sensing: geostationary and Sun-synchronous. Geostationary satellites, such as NASA's GOES and the ESA Meteosat, orbit the Earth at the Equator at the same speed as Earth's rotation and at an altitude of approximately 35,000 km. By matching Earth's orbital speed, geostationary satellites maintain the same view of the Earth's surface at all times and, being at a high altitude, provide near-hemispheric and therefore regular coverage (every 15–30 min). Sun-synchronous satellites, in contrast, are synchronised with the Sun, orbiting the Earth at a much lower altitude (approximately 705 km) and from pole to pole, in such a way that they overpass the Equator at the same local solar time, but a different longitude, on each orbit. The temporal resolution of such sensors is swath-width dependent, ranging from one day (for MODIS, with a swath width of 2330 km) to sixteen (for Landsat-8, with a swath width of 185 km). An additional orbital consideration is that satellites in orbit move at considerable speed (e.g., 27,500 km/h for low Earth orbiting satellites, such as NASA's Terra [29]), thereby rendering image acquisition far from straightforward. To overcome the associated problems, time delay and integration (TDI) technology is used to increase the integration time that a pixel has for viewing the surface, thereby providing a non-blurred image.

**Atmospheric effects:** If accurate radiant emissions data from a volcanic surface are required, then the effect of the atmosphere, and of volcanic gases, that the signal passes through between the surface and the sensor must be accounted for. This is because transmitting gasses may both attenuate and augment radiant signals that pass through. Most infrared bands on sensors used to monitor volcanic activity have been strategically placed in 'atmospheric windows', or portions

of the electromagnetic spectrum with high transmissivity and, hence, low atmospheric absorption (see Figure 5). Even in these windows, however, a small proportion of the signal may be absorbed because volcanic gasses, including water vapour, strongly absorb certain wavelengths. As the atmosphere and volcanic gases also themselves have a temperature, they too emit electromagnetic radiation that contributes to that detected by an observing sensor. A further complication is that a proportion of the atmospheric radiance, and indeed daytime solar radiance, will also be reflected sensor-ward, additionally contributing to the signal detected by satellite sensors. Radiative transfer models are available to simulate such atmospheric effects, and these must be applied to the infrared detections made at a sensor if accurate ground-level emissions data are to be retrieved.

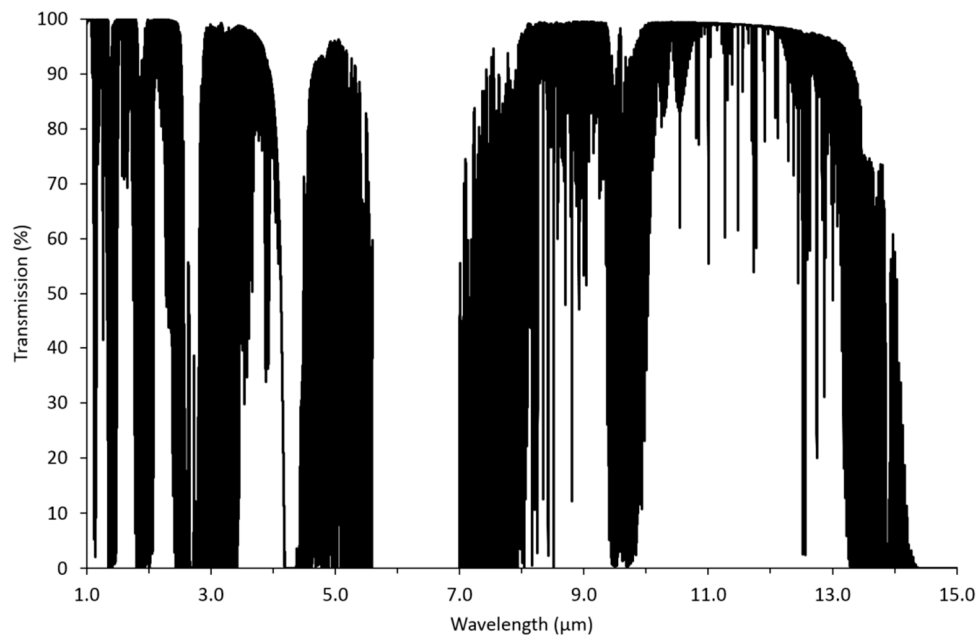


**Figure 5.** Atmospheric transmissivity in the infrared region of the spectrum. Note the limited transmissivity around 6.0  $\mu\text{m}$ , attributable to absorption by water vapour. These data are based on a ‘standard atmosphere’. Source: [30].

**Emissivity:** This is the ratio of energy emitted from a particular body, to that radiated from a perfect emitter (a blackbody) at the same temperature and wavelength; in effect, the term quantifies the radiating efficiency of a surface. An object with an emissivity of 1.0 is a perfect emitter, emitting radiation with 100% efficiency; all other objects emit with less efficiency with the effect that the apparent (or radiance) temperature of such objects, if measured remotely and derived using the Planck equation (Equation (1)), is less than the true kinetic temperature of the object. This means that to derive the true temperature of a volcanic, or indeed any surface, remotely, then its emissivity must be known. The emissivity of volcanic surfaces has been shown to vary widely depending on mineralogy, temperature and the waveband of observation (e.g., it has been shown to be 0.92 in the SWIR bands for cooled andesitic lava at Lascar in Chile [31] and close to 1.0 for the active lava lake at Erta Ale in Ethiopia [8]). Accurate emissivity values are essential, as errors in it have been shown to result in temperature retrieval discrepancies of over 125 K [32].

**Temperature limits:** All sensors used for volcanic thermal signal detection have detection limits. Within these limits, the emissions from a volcanic surface can be detected, but if the signal is too low, it will be missed; and if it is too high, it will saturate the individual pixels of the sensor, rendering quantitative analysis impossible (see Figure 6). Early in the discipline, saturation was identified as one of the key problems in the remote sensing of thermally-anomalous volcanic activity [32], and such issues persist, although the situation is much improved. Determinants of the detection limits include

the dynamic range of the sensor (the range over which radiant signals are detected) and the viewing pixel size (a smaller pixel will saturate at a lower level of radiance when viewing a hot volcanic surface, given that the heated surface components will constitute a greater proportion of the viewing pixel area). In comparing the detection limits of Landsat 8's OLI SWIR bands, with those of its predecessor, Landsat ETM+, the enhanced dynamic range of the former means that temperatures of up to 747.9 K and 570.4 K can be detected without saturation in Bands 6 (1.56–1.66  $\mu\text{m}$ ) and 7 (2.10–2.30  $\mu\text{m}$ ), as compared with those for the corresponding ETM+ bands (724.5 and 552.8 K, respectively) [33]. The problem of saturation was demonstrated in [19], in which it was found that 16% of the volcanic ASTER SWIR scenes analysed displayed saturation, thereby preventing their quantitative analysis. One solution for saturation is the use of varying gain settings to extend the maximum detectable temperatures at the higher end. The SWIR bands of the ASTER sensor, for example, were equipped with low-gain settings for the purpose of volcanic monitoring (a “volcano mode” [34,35]), raising the saturation temperature; in doing so however, it had the effect of reducing sensitivity to cooler surface phenomena [19].

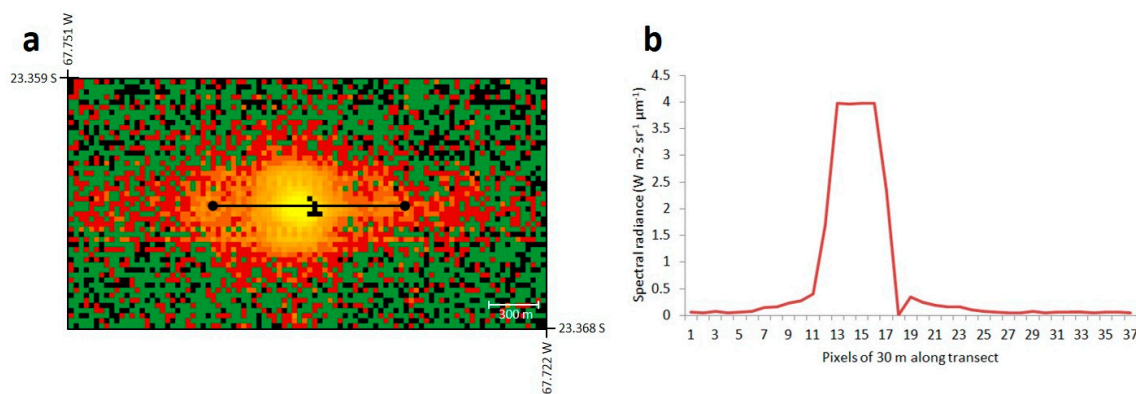


**Figure 6.** (a) Band 9 ASTER (SWIR) nighttime image of Lascar Volcano, Chile, with a transect through the radiant signal; (b) quantification of the signal along the transect in (a). Note that between Pixels 12 and 16, the signal plateaus, indicating saturation. At Pixel 18, the signal is 0  $\text{W m}^{-2} \text{sr}^{-1} \mu\text{m}^{-1}$ , suggesting it has been temporarily disabled because of saturation in adjacent pixels.

#### 4. Historical Perspective on Sensors Used for Volcanic Observation

Infrared remote sensing imagers have been relatively common on orbiting satellites since the early 1960s, with the NOAA TIROS constituting the first operational infrared radiometers in orbit [36]. As technology progressed, so too did the number of platforms launched with infrared imaging capabilities, but it was not until 1968 that many American infrared remote sensing systems were declassified, with data from the TIROS range being the first [37]. Since this period, there has been continuous infrared monitoring of Earth from space [36], with sensors gaining in both spectral and spatial resolution and with data becoming more widely available. The next section will provide a chronology of the discipline, while here, the main satellites and sensors will be presented.

The AVHRR instruments on-board the satellites of the National Oceanic and Atmospheric Administration (NOAA) series were key to the infrared remote sensing of volcanism becoming mainstream. The first AVHRR instrument was launched in 1978, and soon after, their use in volcanic studies began (e.g., [38,39]). The AVHRR instruments have various characteristics useful for the monitoring of volcanic activity, including of most relevance, two infrared bands with a spatial resolution of 1000 m  $\times$  1000 m and, hence, the potential to detect a wide range of thermally-anomalous volcanic phenomena [1]. Each AVHRR orbits the Earth 14 times a day and, with an altitude of 833 km and a swath width of 2399 km, and provides for repeat imagery of the same surface roughly every 12 h (of clear utility in monitoring rapidly changing volcanic events (e.g., [40–42])). Although used less widely today given the availability of newer sensors, AVHRR monitoring of volcanic activity continues (for example, [43]) because of the availability of a long time series of data [44] and NOAA's

policy of retaining two AVHRR satellites in orbit at the same time, effectively enhancing the temporal resolution [36].

In the 1970s, the NASA Landsat programme commenced, although it was not until the 1984 launch of Landsat-5 that functioning SWIR and TIR bands of the Thematic Mapper sensor (TM) were available for thermal studies, possessing spatial resolutions of 30 and 120 m, respectively. The superior spatial resolution of this sensor was achieved with a smaller swath width as compared with AVHRR (185 km versus 2399 km), although this came at the expense of its temporal resolution, which was 16 days. The next successful sensor of the series, on-board Landsat-7, was the Enhanced Thematic Mapper (ETM+), enhanced in terms of its TIR observation capability and superior TIR spatial resolution (60 m). With their higher infrared spatial resolution, the Landsat sensors rapidly became utilized for making more detailed volcanic observations than was possible with AVHRR [45–48], although the reduced temporal resolution meant that the Landsat satellites were less suitable for observing short-lived events. In 2013, the latest in the Landsat series was launched, Landsat-8, as part of the Landsat Data Continuity Mission (LDCM) [49,50]. This satellite was equipped with the Thermal Infrared Sensor (TIRS), possessing two bands with a spatial resolution of 100 m. This reduced spatial resolution, as compared with Landsat-7, was a result of a limited development time [49], but despite this, the TIRS has been shown to acquire accurate volcanic observations, which will, for the foreseeable future, ensure that infrared observations of volcanoes will remain available when MODIS expires [20].

Several geostationary satellites were launched in the 1970s with infrared observing capabilities for meteorological purposes. Of these, the NASA GOES series has been most prolifically used for volcanic observations. The chief advantage of sensors on such systems is that they have an extremely regular image acquisition (four times per hour for GOES and Meteosat), but being geostationary, they are at higher altitude meaning, they have a poorer spatial resolution (4 km for the GOES Imager and 5 km for Meteosat's Visible and Infra-Red Imager (MVIS)). Since 1998, an automated system at the Hawai'i Institute of Geophysics and Planetology has been operational, with the task of processing GOES data for monitoring global volcanic activity, and since this time, various studies have confirmed its utility for extracting volcanic activity chronologies (e.g., [51,52]). SEVERI, the infrared-capable instrument on-board the most recent Meteosat satellites (the Meteosat Second Generation), has similarly been used for such purposes and, indeed, has formed part of an automated volcano monitoring system called HOTSAT, which is implemented, along with MODIS data, when rapid activity detection and monitoring is required [53,54].

In 1986, NASA announced plans for an Earth Observation System (EOS) that would acquire low-Earth orbit observations [55]. Infrared observations fell within the plans, and even prior to its commencement, scientists were optimistic about the role this system could have in the observation of volcanic activity [32]. The EOS satellites were launched from 1999 onwards, and as the data came online, scientists rapidly harnessed them for volcanological applications. The four EOS sensors with infrared observing capabilities were ASTER (on-board the Terra satellite) and MODIS (on-board the Terra and Aqua satellites), as well as the ALI and Hyperion sensors (on-board the EO-1 satellite). Each sensor displayed different characteristics that made them suitable for volcanic observational purposes. ASTER was met with particular optimism within the volcanological community, given that it provided observations in the SWIR (six bands of 30-m resolution) and the TIR (five bands of 90 m), and with a swath width of 60 km and revisit frequency of 16 days, it constituted a follow on to Landsat TM [56–58]. As of 2008, imagery acquired from ASTER's SWIR bands became unusable; the TIR bands remain functioning at the time of writing. Of the other EOS sensors, ALI possessed ten bands from the VNIR to the SWIR, with a spatial resolution of 30 m, while Hyperion shared the 30-m resolution, but possessed a ground-breaking 172 SWIR bands.

Early on, the relatively fine spatial resolution of ASTER's infrared bands was shown to be useful in detecting eruption-precursory thermal anomalies at Chikurachki Volcano, Russia [58], while [19,59] demonstrated that despite its sub-optimal revisit frequency of 16 days, long-term analysis of its data could be used to characterise the behaviour of Shiveluch and Lascar volcanoes, respectively,

with its SWIR and TIR bands showing utility for detecting different thermal components at each volcanic surface. Urai and Ishizuka [60] also demonstrated that within several hours of acquisition, ASTER imagery could be used to estimate the volcanic explosivity index (a scale used to quantify eruption explosiveness) of an eruption, although this relied on ASTER viewing the surface at an appropriate time.

The two identical NASA MODIS instruments were launched three years apart on-board the Terra (1999) and Aqua (2002) platforms, each possessing 16 infrared bands with a spatial resolution of 1000 m and, given a larger pixel size, a larger swath and shorter revisit period (12 h); they had an envisaged design-life of five years [61]. The MODIS sensors have become the most commonly-used sensors for regular and reliable observations of thermally-anomalous volcanic activity. Although their spatial resolution is not ideal, their regular overpasses (up to four times daily when both sensors are considered) have contributed to their widespread use. Various products have been developed that extract and process MODIS thermal data. One such group of products with utility for volcanologists is the MODIS Fire Products, which provide a table of all thermally-anomalous pixels identified within each MODIS scene [62,63]. The MODIS instruments have now been functioning for over 15 years, and this long time series of regular data has allowed scientists to automatically monitor volcanic activity and to determine baseline activity for every active volcano on Earth (e.g., [64–66]).

The latest NASA satellite to have been launched (in 2011) that possesses infrared imaging capabilities is the S-NPP satellite, which features the VIIRS sensor. The S-NPP was launched as an experimental satellite of the Joint Polar Satellite System (JPSS), coordinated by both NASA and NOAA. This system is envisaged as continuing the satellite record of environmental observations, which commenced with AVHRR in the 1970s and continues with MODIS. The VIIRS possesses two sets of bands with infrared detection capabilities: five high resolution imaging (I) bands (375 m) and sixteen moderate (M) resolution bands (750 m), each covering the MIR and TIR portions of the spectrum. To date, there has only been one attempt at using VIIRS data for monitoring volcanic activity, with [67] showing that its detection capabilities are similar, if not superior, to those of MODIS, while a number of studies have similarly confirmed the utility of its infrared bands for monitoring wildfires (e.g., [68,69]).

One final set of satellites that has been used for volcanic observations is what are termed 'small satellites'. Varying definitions exist, but in general, a small satellite is one weighing under 1000 kg, with the small size making them more affordable and potentially commercially mass-producible [70,71]. The first small satellite mission for hot-spot monitoring was the Bi-spectral Infrared Detection (BIRD) mission of the German Aerospace Center (DLR). The BIRD satellite was launched in 2001 and possessed two infrared bands (one MIR and TIR) for identifying hotspots [72]. The satellite entered a relatively low Earth orbit (570 km), with a swath width of 190 km and a pixel size of 370 m × 185 m. Data collected by the sensor (which itself possessed adjustable gain settings) were examined using a customised hotspot detection algorithm. The chief advantages of BIRD were a higher spatial resolution, as compared with sensors, such as MODIS, and the availability of both MIR and TIR detection capabilities (an advantage over ASTER), although these advantages were at the expense of temporal resolution, given its relatively narrow swath [73]. In 2012, a new DLR mission, FireBIRD, commenced, with the micro-Technologieerprobungssträger 1 (TET-1) satellite being launched, possessing two infrared sensors [74]. Although fire observation was the objective of FireBIRD, in late 2014, it imaged the effusion of lava at Stromboli Volcano, Italy, and in this case, its adaptive gain settings meant that while a coincident MODIS image experienced saturation, its data remained unsaturated; and its higher MIR spatial resolution (320 m) provided a relatively more detailed image [75].

Thermal remote sensors utilised for volcanic remote sensing have also been launched by non-U.S. entities. In 1991 and 1995, the ESA launched the European Remote Sensing (ERS) 1 and 2 satellites, each possessing the Along Track Scanning Radiometer (ATSR), which was equipped with MIR and TIR bands and also one SWIR band. In 2002, a third ATSR, the Advanced ATSR (AATSR), was launched following the success of the two earlier versions. The spatial resolution of the ATSR bands was 1000 m × 1000 m, making them less useful for detailed studies than their American counterparts at

the time (those of Landsat TM), but providing an enhanced temporal resolution in the period before MODIS [31]. Given the temporal superiority of ATSR compared to Landsat TM, use of the sensor became common place for several years, and it was used to examine temporal variations in volcanic activity at various locations, including Lascar, Chile [31], Fernandina, Ecuador [76] and Etna, Italy [77], with its surveillance capabilities reviewed in [78]. Findings from the use of ATSR were also used to assess the potential volcanic-utility of the then, not-launched MODIS sensor [79]. Japan also entered the field in 1991 with the launch of the Optical Sensor (OPS) on-board the Japanese Earth Resources Satellite (JERS-1), possessing, for the first time, four high spatial resolution (18 m × 24 m) SWIR bands; it is arguably data from this sensor that highlighted the potential of the shorter-infrared wavelength part of the spectrum for high-temperature surface monitoring [31,80].

## 5. Infrared Remote Sensing of Volcanoes: A History

Given the previous detail concerning the infrared sensors used for monitoring volcanic activity, it will be evident that the discipline has a history of over half a century. As technology has progressed, so have the applications to which the discipline has been applied [81], and these will be highlighted here.

Early infrared radiometer remote sensing surveys were airborne, as opposed to in Earth orbit, with [82] describing this application to Hawaiian volcanoes and producing more detailed and accurate thermal maps than had been possible from land-based observations alone. Later, [83,84] presented radiance maps and detailed how thermal emissions varied spatially at the new Icelandic volcanic islands of Surtsey and Jólnir. Cassinis and Lechi [85,86] also describe aerial volcanic surveys in Italy and at Mount St. Helens, respectively. Gawarecki et al. [87] was the first study to use satellite-acquired infrared data in the detection and monitoring of volcanic activity. However, despite such early experimental endeavours, it remains the case that even today, no satellite sensor has been launched with the sole aim of volcanic infrared monitoring. Volcanologists have been inventive and made use of sensors launched for purposes other than volcanic observation, and unfortunately, nothing seems set to alter this requirement in the near future.

Bonneville et al. [39] stated, in relation to volcanic remote sensing, that “infrared remote-sensing methods remain of limited use” (p. 293), and at the time, this will have done little to encourage take-up of the discipline. This assessment was set to change however, as the discipline soon began to burgeon. Francis and McAllister [88,89] showed how thermal activity at remote Andean volcanoes could be identified without the need for costly and dangerous fieldwork, while [90] took a more global approach, highlighting the general utility of satellite infrared monitoring of volcanoes. Qualitative studies gradually became quantitative, with [91], for example, becoming the first study to consider volcanic surface power emissions as opposed to values of radiance.

Harris [36,81] provides detailed chronologies of the development of the discipline that cannot be bettered here, but in summary, it is shown that during the 1990s, the discipline expanded significantly. The work of Mouginiis-Mark et al. [32] is perhaps responsible for stimulating most interest, by promoting the volcanic utility of the forthcoming NASA Earth Observation System. The initial priority during this period, according to [81], was the identification of ‘hotspots’ and following this, the isolation of temperature distributions (e.g., [45,92,93]). Once perfected in their observations, such studies became more quantitative in their focus and increasingly attempted to relate remote observations to actual phenomena on the ground. Oppenheimer et al. [31,92], for example, were able to identify eruptive periods from a time series of satellite data for Lascar Volcano, Chile, while [42,94] showed how infrared observations could be used to estimate lava effusion rates. It was slowly becoming evident that a reliable and direct relationship existed between the radiant heat emitted from a volcano and the type and intensity of activity displayed at the surface. During this period, the potential seen in the discipline was highlighted in a review paper entitled: ‘Remote Sensing of Active Volcanoes’ [24].

With the small volumes of data coming from the handful of early infrared remote sensors, the early process of detecting the thermal signatures of volcanic activity was largely manual, but between 1995 and 2010, many automated algorithms were developed to detect volcanic thermal anomalies and to avoid false-alarms [81]. Harris et al. [95], for example, developed an algorithm for AVHRR MIR observations, which identified hotspots within a uniformly warm surface, by harnessing the radiance temperature difference between Bands 3 (3.8  $\mu\text{m}$ ) and 4 (10.8  $\mu\text{m}$ ). The concept was that, given that MIR channels (i.e., AVHRR Band 3) are more sensitive to surfaces of magmatic temperature than to those at terrestrial temperatures (see Figure 1), where this temperature difference exceeded a given threshold (applied as 10 K), the surface could be reliably interpreted as displaying a sub-pixel hotspot, which was contributing to the Band 3 signal. Automated processes using such algorithms rapidly developed, including some that were location-specific, such as the Okmok algorithm, which was named after an Alaskan volcano by the same name [42,96]; the Okmok algorithm functioned operationally with AVHRR data, by comparing the temperature of a potentially anomalous pixel to the temperatures of pixels around it; where this temperature difference was shown to be significant, it was automatically determined as anomalous [36].

Steps in automation were also facilitated by improvements in data distribution and storage, with one of the possibilities raised being the monitoring and observation of volcanic activity over wide areas, as opposed to at just one location. Dehn et al. [42] showed how routine AVHRR observations, and the Okmok algorithm, could be used to monitor all volcanoes in the North Pacific, and soon after this, one of the most pervasive and widely-referenced volcanic detection systems was developed called MODVOLC [64,97,98]. This system, which remains operational, works on similar principles to other algorithms: that hotter surfaces will produce a higher spectral radiance at shorter wavelengths, and vice versa. For each MODIS pixel of data, the MODVOLC algorithm calculates a normalized thermal index (NTI) value by differencing the spectral radiant detection between the MIR (Band 22: 3.9  $\mu\text{m}$ ) and TIR (Band 32: 12.00  $\mu\text{m}$ ) bands and then normalizing the result by the sum of these radiances:

$$NTI = \frac{R_{22} - R_{32}}{R_{22} + R_{32}} \quad (2)$$

where  $R_{22}$  and  $R_{32}$  refer to the spectral radiance ( $\text{W m}^{-2} \text{sr}^{-1} \text{m}^{-1}$ ) in MODIS Bands 22 and 32, respectively. If Band 22 is saturated, data from the equivalent, low-gain Band 21 can be used instead. A greater difference between Bands 22 and 32 indicates the presence of a hotter surface, and a threshold is used to identify potential volcanic hotspots [98]. The principle of differencing MIR and TIR signals was also utilised in a later, AATSR-bespoke volcano monitoring system: “Volcanoes Monitoring by Infra-Red”, or VoMIR [99].

Arguably the most sophisticated automated system of the period was the “Autonomous Sciencecraft Experiment System” (later named the “Volcano Sensor Web”) developed for the sensors of the EO-1 spacecraft [100,101]. This system functioned by processing Hyperion SWIR data; if a potential hot surface was identified, then a trigger was generated to re-point the Hyperion sensor appropriately. The system could also be triggered by other sources, such as MODIS, or on-the-ground observations, which re-tasked the satellite to make follow-up observations within two days of notification [100,102]. The effectiveness of this system was demonstrated during the 2010 Eyjafjallajökull eruption, when 50 such observations were made of the erupting volcano over a period of 74 days, ultimately providing data to stakeholders in Iceland to assist in risk and hazard assessments [101].

Despite early recognition of their utility in observing active volcanoes (e.g., [17,90]), few detection algorithms were ever developed for SWIR data. This is because of the greater availability of regular MIR and TIR observations and because MIR and TIR observations were usually available at moderate to low spatial resolution. This latter point meant that large volumes of frequent, wide-area coverage data were obtained that required automated processing, as opposed to more localised, and often ad hoc, SWIR observations [44].

One issue that had to be dealt with from the outset of the discipline was that volcanic surfaces may vary by several-hundred degrees over just a few centimetres [92], and given that 30 m (and often cruder) has been the highest spatial resolution of data available in the infrared, techniques were required to ensure that the data obtained were as accurate as possible. Take a 30-m ASTER or Landsat-8 SWIR pixel for example: the situation on the ground could feasibly match the simulated pixel area of Figure 7, consisting of two (or more) surfaces of different temperature (and consider the possibilities within the 1000 m × 1000 m pixels of AVHRR or MODIS). As such, while radiance detected within one pixel might give an approximate indication of activity on the ground, such a pixel integrated value also hides much information. Given the varying sensitivity of different bands to surfaces of different temperature, any pixel integrated value detected will also be dependent on the band used to image it. For example, again taking the pixel modelled in Figure 7, if viewed in ASTER’s SWIR Band 4, the radiance temperature detected would be 615 K, as compared with 505 K if imaged with ASTER’s Band 9 (see Figure 8). This varying sensitivity is further demonstrated by the wider area of detection in Figure 9 where the Bands 4 and 9 signal detections are compared for the same volcanic surface.

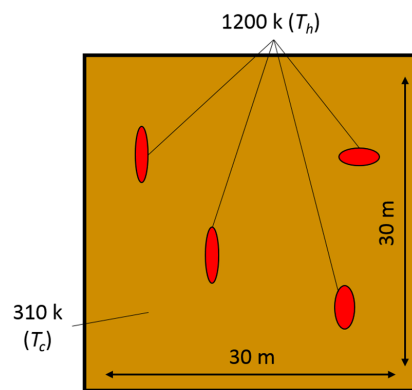


**Figure 7.** A modelled 30-m (e.g., ASTER) pixel, with various hot components at 1200 K and a background surrounding temperature of 310 K. Given these characteristics, the pixel would have an integrated temperature of 615 K at 1.650 μm (ASTER Band 4) and 505 K at 2.395 μm (ASTER Band 9).

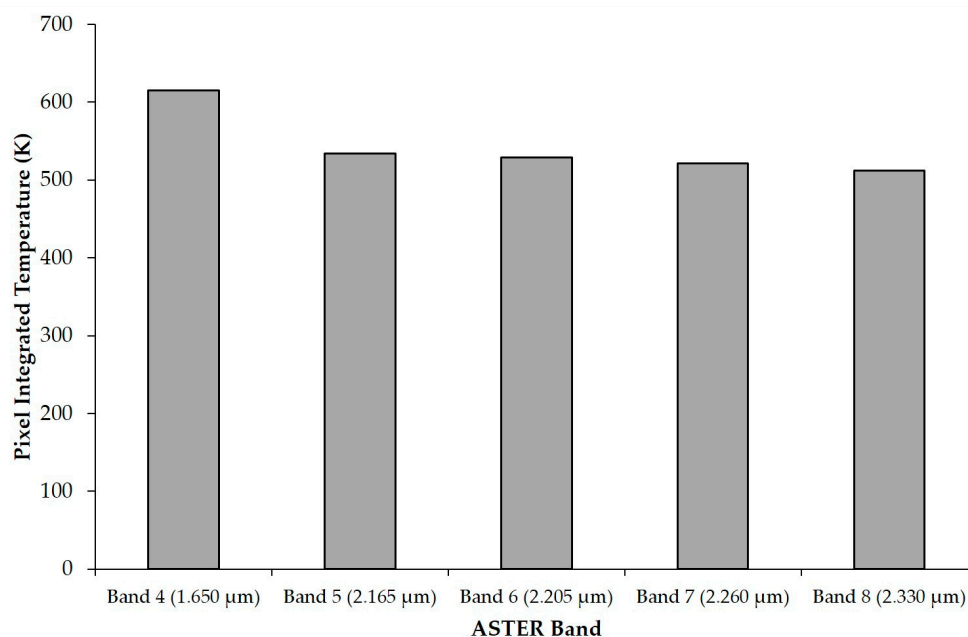


**Figure 8.** The pixel integrated temperature that would be detected by ASTER’s SWIR bands on viewing the modelled surface of Figure 7.

The difference in band sensitivity can be harnessed for volcano monitoring, and this was first documented in [90], using a technique developed in ground breaking studies from 1981: [103,104]. These studies had recognised the distinction between those scenarios in which a whole pixel’s field of view was filled by a thermal anomaly and those in which only a portion of the field of view was thermally anomalous. In the former case, the pixel would measure the full radiance from the surface (e.g., a volcano), and the average temperature of the surface could be calculated; in the latter case, where the anomalous surface consisted of only a portion of the area, the radiance measured would be reduced by this portion, and this would be the case for all observing wavelengths. If the ratio of two pixel values was then taken, it would remain the same in both cases, effectively peak picking the radiance received by the pixel and allowing for an estimation of the sub-pixel two-component thermal structure.

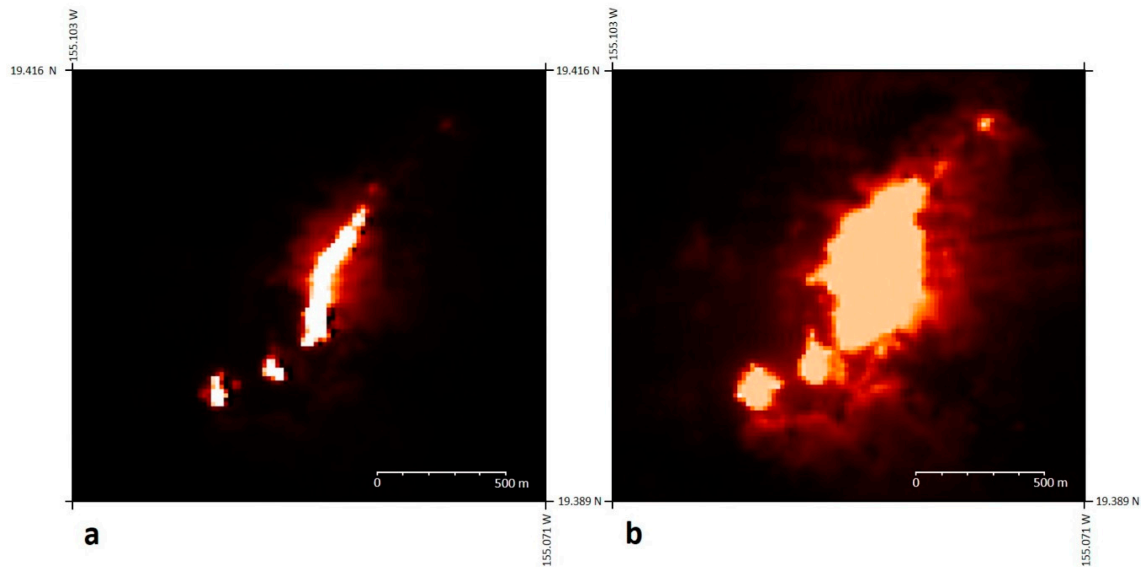


**Figure 9.** Short-wave infrared imagery of the lava flow at Mount Etna, Italy, on 29 July 2007. (a) In ASTER Band 4; (b) in ASTER Band 9. The wider area in (b) demonstrates the detection of radiance from relatively cooler peripheral flow surfaces by Band 9, as compared to the Band 4 image, which only detects the emissions from the lava flow itself.

To characterise a pixel area into two components, non-linear, simultaneous equations, termed the ‘dual-band’ equations, can be used:

$$R_x = P_h L_x(T_h) + [(1 - P_h) L_x(T_c)], \tag{3}$$

and:

$$R_y = P_h L_y(T_h) + [(1 - P_h) L_y(T_c)], \tag{4}$$

where  $R_x$  and  $R_y$  = radiance detected in bands  $x$  and  $y$  ( $W m^{-2} sr^{-1} m^{-1}$ ), adjusted for atmospheric effects and surface emissivity;  $P_h$  = proportion of the pixel occupied by the hotspot;  $L_x(T_h)$  and  $L_y(T_c)$  = spectral radiance ( $L, W m^{-2} sr^{-1} m^{-1}$ ) emitted in a particular band by a surface at temperature  $T_h$  (the hot component) or  $T_c$  (the cooling component), as determined by the Planck function (Equation (1)).

As the ‘dual-band’ method relies on two equations and as there are three unknowns ( $T_h$ ,  $T_c$  and  $P_h$ ), it requires the assumption of either  $T_h$ ,  $T_c$  or  $P_h$ . Volcanologically,  $T_h$  may relate to the temperature of recently erupted lava or an exposed lava lake, while  $T_c$  may relate to the temperature of the surrounding surface unaffected by volcanic processes; both of these can be estimated;  $P_h$ , in contrast, will usually be impossible to estimate accurately and has to be derived. This assumption of two

discrete temperature regions will only be appropriate in some situations and in most cases, will only approximate reality. Furthermore, the technique requires the pixels from which the data are extracted to be completely aligned, therefore precluding use of the technique with data from different sensors.

Determining the temperature and corresponding areas of thermal activity at the surface is useful, but what is arguably more useful from a quantitative point of view is the overall radiant power (i.e., energy) emission. The advantage of an overall power value per pixel is that this value can be summed for all imaging pixels to derive an overall power emission value for the volcanic surface, thus providing a means of monitoring volcanic activity over time and of comparing the activity at different volcanoes. Glaze et al. [91] was one of the first pieces of research to undertake such analysis, based on dual-band equation retrievals, thus setting a standard procedure that was to be reproduced in subsequent studies (e.g., [47,92,105,106]). The radiant power emission, or heat-loss, for an assumed two-component pixel (such as that in Figure 7) can be calculated using the Stefan–Boltzmann law and by calculating the contribution of each component to the overall radiant heat-flux of the pixel:

$$Q = \sigma \varepsilon A [P_h T_h^4 + (1 - P_h) T_c^4] \quad (5)$$

where  $Q$  = radiant power emission (W),  $\sigma$  = Stefan–Boltzmann constant ( $5.67 \times 10^{-8} \text{ W m}^{-2} \text{ K}^{-4}$ ),  $\varepsilon$  = surface emissivity (unit-less) and  $A$  = pixel surface area ( $\text{m}^2$ ).

As multi-spectral infrared imaging capabilities became more widespread, and with higher spatial resolution, the possibility of viewing the surface in more detail, while also allowing for the differentiation of different features within the same surface, became more realistic. Wooster and Rothery [31] showed this by comparing detailed JERS OPS observations of Lascar Volcano, Chile, with those that a corresponding  $1000 \text{ m} \times 1000 \text{ m}$  ATSR pixel would observe. Similar enhancements in observational detail were also demonstrated by [47] in which it was shown that features, such as Hawaiian lava-flow braiding, could be discerned using multispectral and high resolution Landsat ETM+ data.

Experimentations were conducted into using more than two bands of data to better characterize a volcanic surface, with [107], for example, showing that in relation to an active lava flow, a continuum of temperatures is displayed and that as such, a lava-flow surface would be better characterised with 5–7 components. Despite this, and because its outputs are more accurate than assuming one uniform temperature, use of the dual-band technique has persisted. Blackett and Wooster [19] also showed that despite the availability of multiple bands of data, such as the six-SWIR bands of ASTER, the settings of such bands were often sub-optimal for volcanic observational purposes.

In the early 2000s, two data sources remained unexploited: those from the NASA EO-1 satellite's ALI and Hyperion sensors. Their impressive complement of bands meant that these sensors had the potential to discern numerous sub-pixel surfaces for fine and detailed surface characterisations. Wright et al. [108], for example, later demonstrated the utility of such hyper-spectral imagery by using Hyperion data to distinguish various expressions of thermal activity, such as lava lakes, flows and fountains and, indeed, even different lava types, at various volcanoes globally.

As time progressed, long datasets of remotely-sensed infrared imagery had accumulated, extending back to early AVHRR and Landsat observations and coming forward to the NASA-EOS sensors. This provided the possibility of determining the “average”, or baseline radiant emissions, for a particular volcano, and of identifying potential periodicity in these signals and/or chronologies of particular eruptive events. Pergola et al. [109] harnessed the long AVHRR time series for the purpose determining an average infrared signal, both spatially and temporally in volcanic regions, against which volcanic thermal anomalies could be compared and/or identified. The algorithm used to calculate this average was called the Robust AVHRR Technique, and while this technique has been criticised [110], it was later harnessed by [111], but this time with MODIS data, to develop an even more sensitive hot-spot detection algorithm. Wright et al. [66] analysed the entire MODVOLC database, identifying different eruption types and cyclical activity at various volcanoes and calculating the overall heat-flux from all volcanoes active during the operational period of the system. Chronologies

of specific eruptive episodes have also been presented, from [112], which used various sensors to derive a 2003 eruption chronology of Anatahan, Indonesia, to [11,113,114], each of which document eruption chronologies using infrared data for volcanoes in the North Pacific.

Since the end of the last decade, the number of new publications in the discipline has been declining, although the discipline has certainly not stopped making progress. Coppola et al. [15,115], for example, document and validate a new and more sensitive volcanic activity and real-time detection algorithm called MIROVA which uses MODIS MIR data. Additionally, [12] used MODIS TIR data to identify distinct phases of lava dome growth and collapse at Merapi Volcano, Indonesia, and to determine the varied volcanic causes of thermal anomalies detected. Now is perhaps a period of reflection as scientists review data from the past (e.g., [116,117]) and offer suggestions for the design of future infrared imaging satellites (e.g., [118]).

## 6. Prospects for the Future

Sensors used for the infrared monitoring of volcanic activity have immense utility and indeed, have become essential for the monitoring of volcanoes globally. However, there remains a number of shortcomings dictated by the temporal-spatial-spectral resolution trade-off (see Figure 4). These trade-offs have significance when it comes to the remote monitoring of volcanic activity, which, itself, is greatly variable in space, time and intensity. In the case of prolonged eruptive behaviour, such as the incessant effusion of fresh lava from Kilauea, Hawaii, the relatively poor spatial resolution of MODIS, for example, is optimal for accurate and quantifiable observations as it reduces the possibility of image saturation, while its relatively high temporal resolution means that variations in the effusive activity can be well monitored through time. For an unexpected explosive eruption, however, even relatively high temporal resolution imagery (e.g., sub-daily) may be inadequate, resulting in such events often going undetected. Consequently, despite its advantages, infrared remote sensing alone cannot be relied upon for volcanic monitoring, although it constitutes an essential tool for geologists to better understand volcanic processes and for hazard managers to monitor and mitigate associated risks.

Ramsey and Harris [81] argued that 2000–2010 had shown greater progress in the field of volcanic remote sensing than they envisaged for the following decade (up to 2020). Indeed, they discussed the debate that was required to ensure that the subsequent generation of Landsat sensors possessed any infrared sensing capabilities at all [50,81]; the apparent dearth of research over recent years might be explained by several factors, such as that the NASA sensors launched in the late 1990s and early 2000s are coming to the end of their operational lives, while those that remain functional (e.g., Landsat-7 and MODIS) have less than optimal spatial or temporal resolutions. New satellites have been launched with infrared imaging capabilities, such as Landsat-8 and VIIRS on-board S-NPP, but volcanic use of these has been limited, despite showing comparability [20], or indeed improved performance [67]; some retrograde steps, such as the reduction in Landsat-8's infrared spatial resolution, have also been taken. The limited utilisation of these sensors for volcanological studies is by no means a reflection of their potential, and it remains to be seen what new and innovative volcanic observational uses will be derived. At the same time, the body of data from all sensors in orbit continues to grow, providing a repository from which more accurate and representative estimations of volcanic activity might be drawn (e.g., [66]).

In the near future, the provision of infrared volcanic observations will continue, with the successor to the S-NPP, the NASA Joint Polar Satellite System (JPSS 1), due for launch in 2017 and possessing the already proven VIIRS, and with the launch of the ground-breaking Hypsiri sensor, currently planned for 2020 at the earliest [119]. This latter sensor will possess a similar contingent of VNIR and SWIR bands as its predecessor, Hyperion (212 bands between 380 and 2500 nm, although at a reduced spatial resolution of 60 m); additionally, it will have spatially-aligned and higher resolution MIR/TIR imagers (imaging at 60 m in eight bands between 4  $\mu\text{m}$  and 13  $\mu\text{m}$ ). Crucially for Hypsiri, for which one second of operation will produce up to 1 GB of data, the capacity for on-board data processing via an 'Intelligent Payload Module' (IMP) and direct broadcast of a subset of the data [26,28,119] are useful innovations.

On-board automated analyses will have the capacity to identify specific features, for example a volcanic eruption, and once identified, this might trigger further observations of the rapidly changing surface and/or re-task other sensors to make such observations [26,28]. Abrams et al. [119] simulated Hypsiri data with regard to its observation of volcanic activity and showed promising results as compared with ASTER TIR data, given a smaller pixel size (60 m) and higher saturation temperature (700–900 K); its TIR bands will also have an improved temporal resolution (five days at the equator) [28,118]. Hochberg [120] sums up the optimism regarding Hypsiri: “There is no current thermal infrared sensor that combines multiple bands needed for temperature-emissivity separation, a sub-100 m spatial resolution, and a frequent repeat interval with global coverage, which are necessary to answer a wide range of Earth science studies related to surface composition, hydrology, and volcanology” (p. 1). Concerns remain however, as to whether the saturation temperature of the Hypsiri MIR bands will be high enough to prevent saturation over the most radiant lava flows [118].

Another project that shows potential relates to the European Commission’s Earth Observation Programme: Copernicus. As part of this programme, the Sentinel-3 satellite mission is launching two satellites with infrared Earth observation capabilities (Sentinel-3A was launched in early 2016 and Sentinel-3B is due for launch in 2017) to provide continuity to the ATSR and AATSR range. The primary aim of Sentinel-3, and its Sea and Land Surface Temperature Radiometers (SLSTR), is for monitoring ocean and land surface temperatures; however, given their SWIR, MIR and TIR imaging capabilities, they will also provide continuity in volcanic observations. The chief advantages of the SLSTRs are a saturation temperature of 675 K and an equatorial revisit time of half a day (when both satellites are considered); thermal anomaly detection algorithms have been developed and tested for these sensors [121,122].

For the monitoring of volcanic activity, high temporal resolution data, ideally at a sub-daily resolution, such as that provided by geostationary satellites, is particularly useful, and there are prospects that show promise in this regard. The GOES R-Series, for example (the first satellite of which was launched in November 2016), possesses the Advanced Baseline Imager (ABI), which will retain the GOES high temporal resolution while also improving current capabilities, with a superior spatial resolution (0.5–2.0 km) and more bands (including a new SWIR band) [123]. Japan’s equivalent satellites, Himawari-8 (launched in 2015) and -9 (launched in November 2016), each possess a sensor largely comparable in terms of features to the ABI [124]. Similarly, the European Meteosat Third Generation Mission, the first spacecraft of which are due for launch from 2020, will possess more bands on its SEVERI replacement, the Flexible Combined Imager (FCI). FCI’s short wave and near-infrared bands will have a 1-km spatial resolution and a temporal resolution of 10 min, as compared with 15 min at present [125]. These geostationary satellites will also have the capability for rapid scans at times of enhanced activity, and in the case of GOES-R, this may be up to every 30 s [123,124]. Additionally, prospects for the more distant future for instantaneous monitoring are equally promising with Meteosat fourth generation satellites envisioned to be active from around 2035 [126]. These systems will possess an increasingly hyperspectral range of instruments and an even greater spatial and temporal resolution, ideal for monitoring the rapidly changing surfaces associated with volcanoes.

Davies et al. [102] argue that in the future, data from surface sensors, in addition to those from satellites, should form part of any automatic system for identifying volcanic activity. They suggest that had this been the case for the 2010 Eyjafjallajökull eruption, attention would have been focused on the eruption sooner, rather than after the eruption was underway. Ramsey and Harris [81], in contrast, envisage most development in the coming years to relate to small satellites launched privately and at less expense than their larger counterparts.

One of the chief disadvantages of small satellites is that, given their size, and hence narrow swaths, their revisit frequencies are usually sub-optimal for monitoring phenomena that change on short timescales (such as volcanic activity). Small satellites, however, open the possibility that more can be constructed for the same cost as their expensive relatives, resulting in constellations of satellites [127]. Should such constellations be equipped with infrared sensing capabilities, then it would

provide the potential for high spatial and temporal resolution observations of thermally-anomalous volcanic surfaces. China launched one such system, the Small Satellite Constellation for Environment Protection and Disaster Monitoring in 2008, and with its 30-m resolution infrared imaging capabilities, this system has proven useful in observing wildfires [128]. The DLR has also instigated a fire monitoring constellation, FireBIRD, with the first satellite, TET-1, having already shown utility in providing high resolution MIR and TIR imagery of a Strombolian lava flow [75]. The second satellite of the FireBIRD constellation, the Bi-spectral InfraRed Optical System (BIROS), was launched in 2016, and it is envisaged that in total, the FireBIRD constellation will have a three-day revisit period for locations at the Equator [75]. A constellation of multi-spectral infrared VISible-to-thermal IR micro-SATellites (VISIR-SAT) has also been proposed by the DLR, with a spatial resolution of potentially less than 30 m and with one of its aims being: “To predict . . . volcanic hazards through detection of transient thermal phenomena” (p. 1286) [74].

In the last decade, one development in the field of volcanic remote sensing (other than by satellite) has been the use of unmanned aerial vehicles (UAVs) mounted with infrared cameras (e.g., [129]). The chief advantage of such an approach, over that of using satellites, is a higher spatial resolution, given that the UAVs may be a few metres from the surface of interest. However, problems with payload weight, battery power and distance between operator and the hazardous surface have slowed progress in this promising field of study.

In the future, an ideal strategy is for a multi-scale approach, combining the use of high temporal resolution, wide swath spectroradiometers (e.g., MODIS or AVHRR) with higher spatial resolution imagers that focus on high-risk areas. If such systems communicate with each other, events noted at high temporal resolution could be used to trigger higher spatial resolution observations; and the precedence of this has been discussed. One significant prospect in this regard is an ESA Sentinel Convoy, whereby [74] suggests that the VISIR-SAT could be flown with the Sentinel-3 satellites, thus providing high spatial resolution observations of thermal anomalies detected by the coarser resolution, but more widely-viewing, Sentinel range.

Infrared remote sensing of volcanoes has made much progress in little more than half a century. It is essential that this progress is maintained to ensure areas of potential or imminent volcanic hazard are identified for scientists and decision makers. If investment continues in the development of Earth-orbiting infrared remote sensors, then improvements in what scientists can visualize and interpret will continue. Such developments will aid in the understanding of the actual geological phenomena on the ground and in the management of the associated hazards posed to vulnerable communities globally.

**Conflicts of Interest:** The authors declare no conflict of interest.

## References

1. Oppenheimer, C. Review article: Volcanological applications of meteorological satellites. *Int. J. Remote Sens.* **1998**, *19*, 2829–2864. [[CrossRef](#)]
2. Stefan, J. *Über die Beziehung Zwischen der Wärmestrahlung und der Temperatur*; Sitzungsberichte der mathematisch-naturwissenschaftlichen Classe der kaiserlichen Akademie der Wissenschaften: Wien, Austria, 1879; pp. 391–428. (In German)
3. Boltzmann, L. Ableitung des Stefan’schen Gesetzes, betreffend die Abhängigkeit der Wärmestrahlung von der Temperatur aus der electromagnetischen Lichttheorie. *Ann. Phys. Chem.* **1884**, *22*, 291–294. (In German). [[CrossRef](#)]
4. Wien, W. Über die Energieverteilung in Emissionspektrum eines schwarzen Körpers. *Ann. Phys. Chem.* **1896**, *58*, 662–669. (In German). [[CrossRef](#)]
5. Planck, M. Ueber das Gesetz der Energieverteilung im Normalspectrum. *Ann. Phys.* **1901**, *4*, 553–563. (In German). [[CrossRef](#)]

6. Wooster, M.J.; Rothery, D.A. Volcano Surveillance Using Shortwave Infrared Thermal Data from the ERS Along Track Scanning Radiometers. In Proceedings of the ATSR Workshop: Applications of the ERS along Track Scanning Radiometer (ESRIN), Frascati, Italy, 23–25 June 1999.
7. Fink, J.H.; Srivastava, A.; Sylvester, D.; Blaauw, D. *Lava Flows and Domes: Emplacement Mechanisms and Hazard Implications*; Springer: Berlin, Germany, 2008.
8. Oppenheimer, C.; Yirgu, G. Thermal imaging of an active lava lake: Erta 'ale volcano, Ethiopia. *Int. J. Remote Sens.* **2002**, *23*, 4777–4782. [[CrossRef](#)]
9. Carter, A.J.; Girina, O.; Ramsey, M.S.; Demyanchuk, Y.V. ASTER and field observations of the 24 December 2006 eruption of Bezymianny volcano, Russia. *Remote Sens. Environ.* **2008**, *112*, 2569–2577. [[CrossRef](#)]
10. Carter, A.J.; Ramsey, M.S. ASTER- and field-based observations at Bezymianny volcano: Focus on the 11 May 2007 pyroclastic flow deposit. *Remote Sens. Environ.* **2009**, *113*, 2142–2151. [[CrossRef](#)]
11. Wessels, R.L.; Vaughan, R.G.; Patrick, M.R.; Coombs, M.L. High-resolution satellite and airborne thermal infrared imaging of precursory unrest and 2009 eruption at redoubt volcano, Alaska. *J. Volcanol. Geotherm. Res.* **2013**, *259*, 248–269. [[CrossRef](#)]
12. Carr, B.B.; Clarke, A.B.; Vanderkluysen, L. The 2006 lava dome eruption of Merapi volcano (Indonesia): Detailed analysis using MODIS TIR. *J. Volcanol. Geotherm. Res.* **2016**, *311*, 60–71. [[CrossRef](#)]
13. Wright, R.; Pilger, E. Satellite observations reveal little inter-annual variability in the radiant flux from the Mount Erebus lava lake. *J. Volcanol. Geotherm. Res.* **2008**, *177*, 687–694. [[CrossRef](#)]
14. Wright, R.; Pilger, E. Radiant flux from Earth's subaerially erupting volcanoes. *Int. J. Remote Sens.* **2008**, *29*, 6443–6466. [[CrossRef](#)]
15. Coppola, D.; Laiolo, M.; Cigolini, C.; Donne, D.D.; Ripepe, M. Enhanced volcanic hot-spot detection using MODIS IR data. In *Detecting, Modelling and Responding to Effusive Eruptions*; Geological Society of London: London, UK, 2016; pp. 181–205.
16. Rowan, L.C.; Mars, J.C. Lithologic mapping in the mountain pass, California area using advanced Spaceborne thermal emission and reflection Radiometer (ASTER) data. *Remote Sens. Environ.* **2003**, *84*, 350–366. [[CrossRef](#)]
17. Rothery, D.A. The need for volcano monitoring and the ability to detect activity using emitted short wavelength infrared. In Proceedings of the International Geoscience and Remote Sensing Symposium, "Remote Sensing: Moving Toward the 21st Century", Edinburgh, UK, 12–16 September 1988.
18. Pieri, D.; Abrams, M. ASTER watches the world's volcanoes: A new paradigm for volcanological observations from orbit. *J. Volcanol. Geotherm. Res.* **2004**, *135*, 13–28. [[CrossRef](#)]
19. Blackett, M.; Wooster, M.J. Evaluation of SWIR-based methods for quantifying active volcano radiant emissions using NASA EOS-ASTER data. *Geomat. Nat. Hazards Risk* **2011**, *2*, 51–78. [[CrossRef](#)]
20. Blackett, M. Early analysis of Landsat-8 thermal infrared sensor imagery of volcanic activity. *Remote Sens.* **2014**, *6*, 2282–2295. [[CrossRef](#)]
21. Kim, H.; Kim, H.; Lim, H.; Choi, H. Space-Based Earth Observation Activities in South Korea [Space Agencies]. *IEEE Geosci. Remote Sens. Mag.* **2015**, *3*, 34–39. [[CrossRef](#)]
22. Rogalski, A. Infrared detectors: Status and trends. *Prog. Quantum Electron.* **2003**, *27*, 59–210. [[CrossRef](#)]
23. Tupin, F.; Inglada, J.; Nicolas, J.-M. (Eds.) *Remote Sensing Imagery*; Wiley-ISTE: London, UK, 2014.
24. Francis, P.; Rothery, D. Remote sensing of active volcanoes. *Annu. Rev. Earth Planet. Sci.* **2000**, *28*, 81–106. [[CrossRef](#)]
25. Lillesand, T.M.; Kiefer, R.W.; Chipman, J.W.; Lilles, T.M. *Remote Sensing and Image Interpretation*, 5th ed.; Wiley, John & Sons: New York, NY, USA, 2003.
26. NASA. HypsIRI Mission Concept Overview. 2012. Available online: [http://hyspiri.jpl.nasa.gov/downloads/2012\\_Workshop/day1/16\\_HypsIRI\\_Mission\\_Concept\\_Overview-Workshop\\_FY12\\_ULR.pdf](http://hyspiri.jpl.nasa.gov/downloads/2012_Workshop/day1/16_HypsIRI_Mission_Concept_Overview-Workshop_FY12_ULR.pdf) (accessed on 27 December 2016).
27. Chien, S.; Silverman, D.; Davies, A.G.; Mandl, D. Onboard science processing concepts for the HypsIRI mission. *IEEE Intell. Syst.* **2009**, *24*, 12–19. [[CrossRef](#)]
28. Lee, C.M.; Cable, M.L.; Hook, S.J.; Green, R.O.; Ustin, S.L.; Mandl, D.J.; Middleton, E.M. An introduction to the NASA Hyperspectral infraRed Imager (HypsIRI) mission and preparatory activities. *Remote Sens. Environ.* **2015**, *167*, 6–19. [[CrossRef](#)]
29. NASA Earth Observatory. Catalog of Earth Satellite Orbits. Available online: <http://earthobservatory.nasa.gov/Features/OrbitsCatalog/> (accessed on 27 December 2016).

30. Lord, S.D. *NASA Technical Memorandum 103957*; Gemini Observatory: Hilo, HI, USA, 1992; Available online: <http://www.gemini.edu/> (accessed on 7 April 2017).
31. Wooster, M.J.; Rothery, D.A. Thermal monitoring of Lascar volcano, Chile, using infrared data from the along-track scanning radiometer: A 1992–1995 time series. *Bull. Volcanol.* **1997**, *58*, 566–579. [[CrossRef](#)]
32. Mouginiis-Mark, P.; Rowland, S.; Francis, P.; Friedman, T.; Garbeil, H.; Gradie, J.; Self, S.; Wilson, L.; Crisp, J.; Glaze, L.; et al. Analysis of active volcanoes from the earth observing system. *Remote Sens. Environ.* **1991**, *36*, 1–12. [[CrossRef](#)]
33. Morfitt, R.; Barsi, J.; Levy, R.; Markham, B.; Micijevic, E.; Ong, L.; Scaramuzza, P.; Vanderwerff, K. Landsat-8 operational land Imager (OLI) Radiometric performance on-orbit. *Remote Sens.* **2015**, *7*, 2208–2237. [[CrossRef](#)]
34. Yamaguchi, Y.; Kahle, A.B.; Tsu, H.; Kawakami, T.; Pniel, M. Overview of advanced Spaceborne thermal emission and reflection Radiometer (ASTER). *IEEE Trans. Geosci. Remote Sens.* **1998**, *36*, 1062–1071. [[CrossRef](#)]
35. Wright, R.; Rothery, D.A.; Blake, S.; Harris, A.J.L.; Pieri, D.C. Simulating the response of the EOS terra ASTER sensor to high-temperature volcanic targets. *Geophys. Res. Lett.* **1999**, *26*, 1773–1776. [[CrossRef](#)]
36. Harris, A. *Thermal Remote Sensing of Active Volcanoes: A User's Manual*; Cambridge University Press: Cambridge, UK, 2013.
37. Jensen, J.R. *Introductory Digital Image Processing: A Remote Sensing Perspective*, 2nd ed.; Prentice Hall: Upper Saddle River, NJ, USA, 2000.
38. Wiesnet, D.R.; D'Aguanno, J. Thermal imagery of Mount Erebus from the NOAA-6 satellite. *Antarct. J. U. S.* **1982**, *17*, 32–34.
39. Bonneville, A.; Vasseur, G.; Kerr, Y. Satellite Thermal Infrared Observations of Mt. Etna after the 17th March 1981 Eruption. *J. Volcanol. Geotherm. Res.* **1985**, *24*, 293–313. [[CrossRef](#)]
40. Harris, A.J.L.; Blake, S.; Rothery, D.A.; Stevens, N.F. A chronology of the 1991 to 1993 mount Etna eruption using advanced very high resolution radiometer data: Implications for real-time thermal volcano monitoring. *J. Geophys. Res.* **1997**, *102*, 7985. [[CrossRef](#)]
41. Harris, A.J.L.; Flynn, L.P.; Dean, K.; Pilger, E.; Wooster, M.; Okubo, C.; Mouginiis-Mark, P.; Garbeil, H.; Thornber, C.; De la Cruz-Reyna, S.; et al. Real-time satellite monitoring of volcanic hot spots. In *Remote Sensing of Active Volcanism*; Wiley-Blackwell: Hoboken, NJ, USA, 2000; pp. 139–159.
42. Dehn, J.; Dean, K.; Engle, K. Thermal monitoring of north pacific volcanoes from space. *Geology* **2000**, *28*, 755. [[CrossRef](#)]
43. AVO Alaska Volcano Observatory—about AVO—Operations. 2014. Available online: <https://www.avo.alaska.edu/about/operations> (accessed on 30 September 2016).
44. Blackett, M. Review of the utility of infrared remote sensing for detecting and monitoring volcanic activity with the case study of shortwave infrared data for Lascar volcano from 2001–2005. In *Geological Society, London, Special Publications*; Geological Society of London: London, UK, 2013; Volume 380, pp. 107–135.
45. Flynn, L.P.; Mouginiis-Mark, P.J.; Horton, K.A. Distribution of thermal areas on an active lava flow field: Landsat observations of Kilauea, Hawaii, July 1991. *Bull. Volcanol.* **1994**, *56*, 284–296. [[CrossRef](#)]
46. Flynn, L.P.; Harris, A.J.L.; Rothery, D.A.; Oppenheimer, C. High-spatial-resolution thermal remote sensing of active volcanic features using Landsat and hyperspectral data. In *Remote Sensing of Active Volcanism*; Wiley-Blackwell: Hoboken, NJ, USA, 2000; pp. 161–177.
47. Flynn, L.P.; Harris, A.J.L.; Wright, R. Improved identification of volcanic features using Landsat 7 ETM+. *Remote Sens. Environ.* **2001**, *78*, 180–193. [[CrossRef](#)]
48. Lombardo, V.; Buongiorno, M.F.; Pieri, D.; Merucci, L. Differences in Landsat TM derived lava flow thermal structures during summit and flank eruption at mount Etna. *J. Volcanol. Geotherm. Res.* **2004**, *134*, 15–34. [[CrossRef](#)]
49. Irons, J.R.; Dwyer, J.L. An overview of the Landsat data continuity mission. *Proc. SPIE* **2010**, 7695. [[CrossRef](#)]
50. Irons, J.R.; Dwyer, J.L.; Barsi, J.A. The next Landsat satellite: The Landsat data continuity mission. *Remote Sens. Environ.* **2012**, *122*, 11–21. [[CrossRef](#)]
51. Harris, A.J.L.; Keszthelyi, L.; Flynn, L.P.; Mouginiis-Mark, P.J.; Thornber, C.; Kauahikaua, J.; Sherrod, D.; Trusdell, F.; Sawyer, M.W.; Flament, P. Chronology of the episode 54 eruption at Kilauea volcano, Hawaii, from GOES-9 satellite data. *Geophys. Res. Lett.* **1997**, *24*, 3281–3284. [[CrossRef](#)]
52. Harris, A.J.L.; Pilger, E.; Flynn, L.P.; Garbeil, H.; Mouginiis-Mark, P.J.; Kauahikaua, J.; Thornber, C. Automated, high temporal resolution, thermal analysis of Kilauea volcano, Hawai'i, using GOES satellite data. *Int. J. Remote Sens.* **2001**, *22*, 945–967. [[CrossRef](#)]

53. Ganci, G.; Vicari, A.; Fortuna, L.; Del Negro, C. The HOTSAT volcano monitoring system based on combined use of SEVIRI and MODIS multispectral data. *Ann. Geophys.* **2011**, *54*. [[CrossRef](#)]
54. Ganci, G.; Bilotta, G.; Cappello, A.; Herault, A.; Negro, C.D. HOTSAT. In *Detecting, Modelling and Responding to Effusive Eruptions*; Geological Society of London: London, UK, 2016; pp. 207–221.
55. NASA. Earth Observing System. Data and Information System. Report of the EOS Data Panel. Available online: <http://ntrs.nasa.gov/archive/nasa/casi.ntrs.nasa.gov/19860021622.pdf> (accessed on 1 October 2016).
56. Pieri, D.C.; Crisp, J.; Kahle, A.B. Observing Volcanism and Other Transient Phenomena with ASTER. *J. Remote Sens. Soc. Jpn.* **1995**, *15*, 56–61.
57. Abrams, M. The advanced Spaceborne thermal emission and reflection Radiometer (ASTER): Data products for the high spatial resolution imager on NASA's terra platform. *Int. J. Remote Sens.* **2000**, *21*, 847–859. [[CrossRef](#)]
58. Pieri, D.; Abrams, M. ASTER observations of thermal anomalies preceding the April 2003 eruption of Chikurachki volcano, Kurile islands, Russia. *Remote Sens. Environ.* **2005**, *99*, 84–94. [[CrossRef](#)]
59. Carter, A.; Ramsey, M. Long-term volcanic activity at Shiveluch volcano: Nine years of ASTER Spaceborne thermal infrared observations. *Remote Sens.* **2010**, *2*, 2571–2583. [[CrossRef](#)]
60. Urai, M.; Ishizuka, Y. Advantages and challenges of space-borne remote sensing for volcanic Explosivity index (VEI): The 2009 eruption of Sarychev peak on Matua Island, Kuril Islands, Russia. *J. Volcanol. Geotherm. Res.* **2011**, *208*, 163–168. [[CrossRef](#)]
61. LP DAAC: NASA Land Data Products and Services. Available online: [https://lpdaac.usgs.gov/15\\_years\\_terra\\_modis](https://lpdaac.usgs.gov/15_years_terra_modis) (accessed on 1 October 2016).
62. Kaufman, Y.J.; Justice, C.O.; Flynn, L.P.; Kendall, J.D.; Prins, E.M.; Giglio, L.; Ward, D.E.; Menzel, W.P.; Setzer, A.W. Potential global fire monitoring from EOS-MODIS. *J. Geophys. Res. Atmos.* **1998**, *103*, 32215–32238. [[CrossRef](#)]
63. Justice, C.; Giglio, L.; Korontzi, S.; Owens, J.; Morisette, J.; Roy, D.; Descloitres, J.; Alleaume, S.; Petitcolin, F.; Kaufman, Y. The MODIS fire products. *Remote Sens. Environ.* **2002**, *83*, 244–262. [[CrossRef](#)]
64. Wright, R.; Flynn, L.; Garbeil, H.; Harris, A.; Pilger, E. Automated volcanic eruption detection using MODIS. *Remote Sens. Environ.* **2002**, *82*, 135–155. [[CrossRef](#)]
65. Wright, R.; Flynn, L.P. Space-based estimate of the volcanic heat flux into the atmosphere during 2001 and 2002. *Geology* **2004**, *32*, 189. [[CrossRef](#)]
66. Wright, R.; Blackett, M.; Hill-Butler, C. Some observations regarding the thermal flux from Earth's erupting volcanoes for the period of 2000 to 2014. *Geophys. Res. Lett.* **2015**, *42*, 282–289. [[CrossRef](#)]
67. Blackett, M. An initial comparison of the thermal anomaly detection products of MODIS and VIIRS in their observation of Indonesian volcanic activity. *Remote Sens. Environ.* **2015**, *171*, 75–82. [[CrossRef](#)]
68. Justice, C.O.; Román, M.O.; Csiszar, I.; Vermote, E.F.; Wolfe, R.E.; Hook, S.J.; Friedl, M.; Wang, Z.; Schaaf, C.B.; Miura, T.; et al. Land and cryosphere products from Suomi NPP VIIRS: Overview and status. *J. Geophys. Res. Atmos.* **2013**, *118*, 9753–9765. [[CrossRef](#)] [[PubMed](#)]
69. Csiszar, I.; Schroeder, W.; Giglio, L.; Ellicott, E.; Vadrevu, K.P.; Justice, C.O.; Wind, B. Active fires from the Suomi NPP visible infrared imaging Radiometer suite: Product status and first evaluation results. *J. Geophys. Res. Atmos.* **2014**, *119*, 803–816. [[CrossRef](#)]
70. Barnhart, D.J.; Vladimirova, T.; Sweeting, M.N. Very-small-satellite design for distributed space missions. *J. Spacecr. Rockets* **2007**, *44*, 1294–1306. [[CrossRef](#)]
71. Sandau, R. Small Satellite Missions. In *Advances in Photogrammetry, Remote Sensing and Spatial Information Sciences: 2008 ISPRS Congress Book*; Li, Z., Chen, J., Baltsavias, E., Eds.; CRC Press: Cullompton, UK, 2008.
72. Brieß, K.; Bärwald, W.; Gerlich, T.; Jahn, H.; Lura, F.; Studemund, H. The DLR small satellite mission BIRD. *Acta Astronaut.* **2000**, *46*, 111–120. [[CrossRef](#)]
73. Zhukov, B.; Lorenz, E.; Oertel, D.; Wooster, M.; Roberts, G. Spaceborne detection and characterization of fires during the bi-spectral infrared detection (BIRD) experimental small satellite mission (2001–2004). *Remote Sens. Environ.* **2006**, *100*, 29–51. [[CrossRef](#)]
74. Ruecker, G.; Menz, G.; Heinemann, S.; Hartmann, M.; Oertel, D. VISIR-SAT—A Prospective micro-satellite based multi-spectral thermal mission for land applications. In *Proceedings of the ISPRS International Archives of the Photogrammetry, Remote Sensing and Spatial Information Sciences*, Berlin, Germany, 11–15 May 2015; Volume XL-7/W3, pp. 1283–1289.

75. Zakšek, K.; Hort, M.; Lorenz, E. Satellite and ground based thermal observation of the 2014 effusive eruption at Stromboli volcano. *Remote Sens.* **2015**, *7*, 17190–17211. [CrossRef]
76. Wooster, M.J.; Rothery, D.A. Time-series analysis of effusive volcanic activity using the ERS along track scanning radiometer: The 1995 eruption of Fernandina volcano, Galápagos Islands. *Remote Sens. Environ.* **1997**, *62*, 109–117. [CrossRef]
77. Rothery, D.; Coltelli, M.; Pieri, D.; Wooster, M.; Wright, R. Documenting surface magmatic activity at Mount Etna using ATSR remote sensing. *Bull. Volcanol.* **2001**, *63*, 387–397.
78. Wooster, M.J.; Rothery, D.A. A Review of Volcano Surveillance Applications Using the ATSR Instrument Series. *Adv. Environ. Monit. Model.* **2002**, *1*, 97–123.
79. Wooster, M.J.; Rothery, D.A.; Kaneko, T. Geometric considerations for the remote monitoring of volcanoes: Studies of lava domes using ATSR and the implications for MODIS. *Int. J. Remote Sens.* **1998**, *19*, 2585–2591. [CrossRef]
80. Dennis, A.M.; Harris, A.J.L.; Carlton, R.W.; Francis, P.W.; Rothery, D.A. Cover the 1993 Lascar pyroclastic flow imaged by JERS-1. *Int. J. Remote Sens.* **1996**, *17*, 1975–1980. [CrossRef]
81. Ramsey, M.S.; Harris, A.J.L. Volcanology 2020: How will thermal remote sensing of volcanic surface activity evolve over the next decade? *J. Volcanol. Geotherm. Res.* **2013**, *249*, 217–233. [CrossRef]
82. Fisher, W.A.; Mozham, R.M.; Polcyn, F.; Landis, G.H. Infrared surveys of Hawaiian Volcanoes. *Science* **1964**, *146*, 733–742. [CrossRef] [PubMed]
83. Williams, R.S., Jr.; Friedman, J.D.; Thórarinnsson, S.; Sigurgeirsson, T.; Pálmason, G. Analysis of 1966 Infrared Imagery of Surtsey, Iceland. Surtsey Research Progress Report IV. 1968. Available online: [http://www.surtsey.is/SRS\\_public/1968-IV/1968\\_IV\\_5\\_04.pdf](http://www.surtsey.is/SRS_public/1968-IV/1968_IV_5_04.pdf) (accessed on 7 April 2017).
84. Friedman, J.D.; Williams, R.S., Jr.; Þórarinnsson, S.; Pálmason, G. Infrared Emission from Kverkfjöll Subglacial Volcanic and Geothermal Area, Iceland. *Jökull* **1972**, *22*, 27–43.
85. Cassinis, R.; Lechi, G.M. The Use of Infrared Radiometry in Geothermal Areas. In *Physical Volcanology (Development in Solid Earth Geophysics)*; Civetta, L., Ed.; Elsevier: Amsterdam, The Netherlands, 1974.
86. Kieffer, H.H.; Frank, D.; Friedman, J.D. Thermal infrared surveys at Mount St. Helens—Observations prior to the eruption of May 18. In *The 1980 Eruptions of Mount St. Helens, Washington*; Lipman, P.W., Mullineaux, D.R., Eds.; USGS Professional Paper 1250; U.S. Government Printing Office: Washington, DC, USA, 1981; pp. 257–277.
87. Gawarecki, S.J.; Lyon, R.J.P.; Nordberg, W. Infrared spectral returns and imagery of the Earth from space and their application to geological problems: Scientific experiments for manned orbital flight. *Am. Astronaut. Soc. Sci. Technol.* **1965**, *4*, 13–133.
88. Francis, P.W.; McAllister, R. Volcanology from space: Using Landsat thematic Mapper data in the central Andes. *Eos Trans. Am. Geophys. Union* **1986**, *67*, 170. [CrossRef]
89. Francis, P.W.; Rothery, D.A. Using the Landsat Thematic Mapper to detect and monitor active volcanoes: An example from Lascar volcano, Northern Chile. *Geology* **1987**, *15*, 614–617. [CrossRef]
90. Rothery, D.A.; Francis, P.W.; Wood, C.A. Volcano monitoring using short wavelength infrared data from satellites. *J. Geophys. Res.* **1988**, *93*, 7993. [CrossRef]
91. Glaze, L.; Francis, P.W.; Rothery, D.A. Measuring thermal budgets of active volcanoes by satellite remote sensing. *Nature* **1989**, *338*, 144–146. [CrossRef]
92. Oppenheimer, C.; Francis, P.W.; Rothery, D.A.; Carlton, R.W.T.; Glaze, L.S. Infrared image analysis of volcanic thermal features: Lascar volcano, Chile, 1984–1992. *J. Geophys. Res.* **1993**, *98*, 4269. [CrossRef]
93. Flynn, L.P.; Mouginiis-Mark, P.J. Temperature of an active lava channel from spectral measurements, Kilauea volcano, Hawaii. *Bull. Volcanol.* **1994**, *56*, 297–301. [CrossRef]
94. Harris, A.J.L.; Flynn, L.P.; Keszthelyi, L.; Mouginiis-Mark, P.J.; Rowland, S.K.; Resing, J.A. Calculation of lava effusion rates from Landsat TM data. *Bull. Volcanol.* **1998**, *60*, 52–71. [CrossRef]
95. Harris, A.J.L.; Vaughan, R.A.; Rothery, D.A. Volcano detection and monitoring using AVHRR data: The Krafla eruption, 1984. *Int. J. Remote Sens.* **1995**, *16*, 1001–1020. [CrossRef]
96. Dean, K.; Servilla, M.; Roach, A.; Foster, B.; Engle, K. Satellite monitoring of remote volcanoes improves study efforts in Alaska. *Eos Trans. Am. Geophys. Union* **1998**, *79*, 413. [CrossRef]
97. Flynn, L.P.; Wright, R.; Garbeil, H.; Harrism, A.J.L.; Pilger, E. A global thermal alert system using MODIS: Initial results from 2000–2001. *Adv. Environ. Monit. Model.* **2002**, *1*, 37–69.

98. Wright, R.; Flynn, L.P.; Garbeil, H.; Harris, A.J.; Pilger, E. MODVOLC: Near-real-time thermal monitoring of global volcanism. *J. Volcanol. Geotherm. Res.* **2004**, *135*, 29–49. [[CrossRef](#)]
99. Colin, O.; Rubio, M.; Landart, P.; Mathot, E. VoMIR: Over 300 volcanoes monitored in near real-time by AATSR. In Proceedings of the Envisat Symposium 2007, Montreux, Switzerland, 23–27 April 2007.
100. Davies, A.G.; Chien, S.; Baker, V.; Doggett, T.; Dohm, J.; Greeley, R.; Ip, F.; Castan˜o, R.; Cichy, B.; Rabideau, G.; et al. Monitoring active volcanism with the autonomous Sciencecraft experiment on EO-1. *Remote Sens. Environ.* **2006**, *101*, 427–446. [[CrossRef](#)]
101. Davies, A.G.; Chien, S.; Doubleday, J.; Tran, D.; Thordarson, T.; Gudmundsson, M.T.; Höskuldsson, Á.; Jakobsdóttir, S.S.; Wright, R.; Mandl, D. Observing Iceland’s Eyjafjallajökull 2010 eruptions with the autonomous NASA volcano sensor web. *J. Geophys. Res. Solid Earth* **2013**, *118*, 1936–1956. [[CrossRef](#)]
102. Davies, A.G.; Chien, S.; Tran, D.Q.; Doubleday, J. Onboard processing of multispectral and hyperspectral data of volcanic activity for future earth-orbiting and planetary missions. In Proceedings of the 2010 IEEE International Geoscience and Remote Sensing Symposium, Honolulu, HI, USA, 25–30 July 2010.
103. Dozier, J. A method for satellite identification of surface temperature fields of subpixel resolution. *Remote Sens. Environ.* **1981**, *11*, 221–229. [[CrossRef](#)]
104. Matson, M.; Dozier, J. Identification of Subresolution High Temperature Sources Using a Thermal IR Sensor. *Photogramm. Eng. Remote Sens.* **1981**, *47*, 1311–1318.
105. Oppenheimer, C. Lava flow cooling estimated from Landsat thematic Mapper infrared data: The Lonquimay eruption (Chile, 1989). *J. Geophys. Res. Solid Earth* **1991**, *96*, 21865–21878. [[CrossRef](#)]
106. Wooster, M.J.; Wright, R.; Blake, S.; Rothery, D.A. Cooling mechanisms and an approximate thermal budget for the 1991–1993 Mount Etna lava flow. *Geophys. Res. Lett.* **1997**, *24*, 3277–3280. [[CrossRef](#)]
107. Wright, R.; Flynn, L.P. On the retrieval of lava-flow surface temperatures from infrared satellite data. *Geology* **2003**, *31*, 893. [[CrossRef](#)]
108. Wright, R.; Glaze, L.; Baloga, S.M. Constraints on determining the eruption style and composition of terrestrial lavas from space. *Geology* **2011**, *39*, 1127–1130. [[CrossRef](#)]
109. Pergola, N.; Marchese, F.; Tramutoli, V. Automated detection of thermal features of active volcanoes by means of infrared AVHRR records. *Remote Sens. Environ.* **2004**, *93*, 311–327. [[CrossRef](#)]
110. Blackett, M.; Wooster, M.J.; Malamud, B.D. Exploring land surface temperature earthquake precursors: A focus on the Gujarat (India) earthquake of 2001. *Geophys. Res. Lett.* **2011**, *38*, L15303. [[CrossRef](#)]
111. Koepfen, W.C.; Pilger, E.; Wright, R. Time series analysis of infrared satellite data for detecting thermal anomalies: A hybrid approach. *Bull. Volcanol.* **2010**, *73*, 577–593. [[CrossRef](#)]
112. Wright, R.; Carn, S.A.; Flynn, L.P. A satellite chronology of the May–June 2003 eruption of Anatahan volcano. *J. Volcanol. Geotherm. Res.* **2005**, *146*, 102–116. [[CrossRef](#)]
113. Rose, S.; Ramsey, M. The 2005 eruption of Kliuchevskoi volcano: Chronology and processes derived from ASTER spaceborne and field-based data. *J. Volcanol. Geotherm. Res.* **2009**, *184*, 367–380. [[CrossRef](#)]
114. Rybin, A.; Chibisova, M.; Webley, P.; Steensen, T.; Izbekov, P.; Neal, C.; Realmuto, V. Satellite and ground observations of the June 2009 eruption of Sarychev peak volcano, Matua island, central Kuriles. *Bull. Volcanol.* **2011**, *73*, 1377–1392. [[CrossRef](#)]
115. Coppola, D.; Laiolo, M.; Cigolini, C. Fifteen years of thermal activity at Vanuatu’s volcanoes (2000–2015) revealed by MIROVA. *J. Volcanol. Geotherm. Res.* **2015**, *322*, 6–19. [[CrossRef](#)]
116. Wright, R. MODVOLC. In *Detecting, Modelling and Responding to Effusive Eruptions*; Geological Society of London: London, UK, 2015; pp. 23–53.
117. Flower, V.J.B.; Carn, S.A.; Wright, R. The impact of satellite sensor viewing geometry on time-series analysis of volcanic emissions. *Remote Sens. Environ.* **2016**, *183*, 282–293. [[CrossRef](#)]
118. Realmuto, V.J.; Dennison, P.E.; Foote, M.; Ramsey, M.S.; Wooster, M.J.; Wright, R. Specifying the saturation temperature for the HypsIRI 4- $\mu\text{m}$  channel. *Remote Sens. Environ.* **2015**, *167*, 40–52. [[CrossRef](#)]
119. Abrams, M.; Pieri, D.; Realmuto, V.; Wright, R. Using EO-1 Hyperion data as HypsIRI preparatory data sets for Volcanology applied to Mt Etna, Italy. *IEEE J. Sel. Top. Appl. Earth Obs. Remote Sens.* **2013**, *6*, 375–385. [[CrossRef](#)]
120. Hochberg, E.J.; Roberts, D.A.; Dennison, P.E.; Hulley, G.C. Special issue on the Hyperspectral infrared Imager (HypsIRI): Emerging science in terrestrial and aquatic ecology, radiation balance and hazards. *Remote Sens. Environ.* **2015**, *167*, 1–5. [[CrossRef](#)]

121. Wooster, M.J.; Xu, W.; Nightingale, T. Sentinel-3 SLSTR active fire detection and FRP product: Pre-launch algorithm development and performance evaluation using MODIS and ASTER datasets. *Remote Sens. Environ.* **2012**, *120*, 236–254. [[CrossRef](#)]
122. User Guides—Sentinel-3 SLSTR—Heritage—Sentinel. Available online: <https://earth.esa.int/web/sentinel/user-guides/sentinel-3-slstr/overview/heritage> (accessed on 1 October 2016).
123. Schmit, T.J.; Gunshor, M.M.; Menzel, W.P.; Gurka, J.J.; Li, J.; Bachmeier, A.S. Introducing the next-generation Advanced Baseline Imager on GOES-R. *Bull. Am. Meteorol. Soc.* **2005**, *86*, 1079–1096. [[CrossRef](#)]
124. Takahashi, M. Status of Next Generation Japanese Geostationary Meteorological Satellites Himawari-8/9 and Their Products. In Proceedings of the NOAS Satellite Science Week, GOES-R Algorithm Working Group, Kansas City, MO, USA, 30 April–4 May 2012.
125. Kinter, H.; Just, D.; Mullet, B. Meteosat third generation navigation approach. In Proceedings of the 22nd International Symposium on Space Flight Dynamics, São José dos Campos, Brazil, 28 February–4 March 2011.
126. Puschell, J.; Cook, L.; Shaham, Y.; Makowski, M.; Silny, J. System engineering studies for advanced geosynchronous remote sensors: Some initial thoughts on the 4th generation. *Proc. SPIE* **2008**, *7087*. [[CrossRef](#)]
127. Xue, Y.; Li, Y.; Guang, J.; Zhang, X.; Guo, J. Small satellite remote sensing and applications—History, current and future. *Int. J. Remote Sens.* **2008**, *29*, 4339–4372. [[CrossRef](#)]
128. Liu, S.; Fan, Y.; Gao, M. Natural disaster reduction applications of the Chinese small satellite constellation for environment and disaster monitoring and forecasting. *Proc. SPIE* **2013**, *8921*. [[CrossRef](#)]
129. Sheng, H.; Chao, H.; Coopmans, C.; Han, J.; McKee, M.; Chen, Y. Low-cost UAV-based thermal infrared remote sensing: Platform, calibration and applications. In Proceedings of the 2010 IEEE/ASME International Conference on Mechatronic and Embedded Systems and Applications, Qingdao, China, 15–17 July 2010; pp. 38–43.



© 2017 by the author. Licensee MDPI, Basel, Switzerland. This article is an open access article distributed under the terms and conditions of the Creative Commons Attribution (CC BY) license (<http://creativecommons.org/licenses/by/4.0/>).